Titre: Title:	3D-Printed Terahertz Demultiplexers
Auteur: Author:	Babak Yahyapour
Date:	2025
Type:	Mémoire ou thèse / Dissertation or Thesis
Référence: Citation:	Yahyapour, B. (2025). 3D-Printed Terahertz Demultiplexers [Mémoire de maîtrise, Polytechnique Montréal]. PolyPublie. https://publications.polymtl.ca/71474/

POLYTECHNIQUE MONTRÉAL
affiliée à l'Université de Montréal

3D-PRINTED TERAHERTZ DEMULTIPLEXERS

BABAK YAHYAPOUR
Département de génie physique

Mémoire présenté en vue de l'obtention du diplôme de *Maîtrise ès sciences appliquées*
Génie physique

Décembre 2025

POLYTECHNIQUE MONTRÉAL
affiliée à l'Université de Montréal

Ce mémoire intitulé :

3D-PRINTED TERAHERTZ DEMULTIPLEXERS

présenté par **Babak YAHYAPOUR**
en vue de l'obtention du diplôme de *Maîtrise ès sciences appliquées*
a été dûment accepté par le jury d'examen constitué de :

Sean MOLESKY, président
Maksim SKOROBOGATIY, membre et directeur de recherche
Nicolas GODBOUT, membre

DEDICATION

To my beloved partner, and our parents, for their unconditional love and support.

ACKNOWLEDGEMENTS

I would like to express my deepest gratitude to Prof. Maksim Skorobogatiy for his invaluable guidance and support throughout my academic journey. Under his supervision, I have learned far more than I could have ever imagined. These past two years have been filled with discovery, and I am profoundly thankful to him for welcoming me into his research group and for providing an environment in which I was able to grow and thrive.

I would also like to acknowledge everyone who contributed, directly or indirectly, to the completion of this thesis. In particular, I thank Guofu Xu and Roya Gachiloo, whose support and insights were greatly appreciated. I am equally grateful to my colleagues in the office and the laboratory for the many enjoyable moments we shared. Our numerous fruitful discussions were a constant source of inspiration and learning.

Finally, I dedicate this work to my family, my parents, who raised me in an atmosphere of curiosity and a love for learning, and my beloved partner, whose kindness, care, and unwavering support motivated me to push my limits and strive for excellence.

RÉSUMÉ

La demande croissante en bande passante sans fil nécessite l'exploration de la bande de fréquence térahertz (THz) (0,1-10 THz) comme nouvelle frontière pour les technologies de communication. Le multiplexage par division de longueur d'onde (WDM) est une technologie clé pour augmenter la capacité des systèmes de communication THz, pour lesquels les démultiplexeurs intégrés (Demux) sont des composants essentiels. Cependant, la fabrication de tels dispositifs repose souvent sur des processus complexes et coûteux en photonique sur silicium, qui ne sont pas adaptés au prototypage rapide. Cette thèse présente une approche novatrice et rentable pour la conception et la fabrication de démultiplexeurs THz haute performance à l'aide de la fabrication additive (impression 3D).

Dans cette approche, nous utilisons une imprimante Fused Deposition Modeling (FDM) à deux buses pour créer des circuits en polypropylène suspendus dans l'air, tirant parti du contraste élevé de l'indice de réfraction pour des dispositifs guidés compacts et à faibles pertes. Les composants clés sont les filtres à réseau de Bragg à guide d'onde couplé latéralement, qui ont été optimisés numériquement à l'aide de la modélisation par éléments finis pour fonctionner dans la bande de 120 à 165 GHz. Nous avons réussi à fabriquer trois filtres distincts avec des canaux de coupure centrés sur 138 GHz, 142 GHz et 146 GHz, chacun offrant une largeur de bande d'environ 5 GHz et un espacement inter-canaux d'environ 4 GHz. La caractérisation expérimentale a démontré la réussite du démultiplexage de trois canaux avec des débits de données allant jusqu'à 6 Gbps, tout en maintenant un taux d'erreur binaire (BER) inférieur à la limite de correction d'erreur avant. Les spectres mesurés ont montré une forte suppression des lobes secondaires et une largeur de bande des ports de coupure plus large (6 GHz) que celle simulée (4 GHz), bien que les amplitudes de transmission aient été légèrement plus faibles (0,5-0,6 contre 0,8 prévues) en raison des pertes de diffusion liées aux structures de support. De plus, nous avons démontré l'intégration de ces filtres dans des démultiplexeurs fonctionnels à quatre canaux utilisant à la fois des configurations planaires (horizontales) et plus compactes en dehors du plan (verticales), connectées via une technique de soudure à faibles pertes. Ce travail établit l'impression 3D comme une plateforme de fabrication viable et flexible pour les circuits intégrés THz complexes. La capacité de prototypage rapide démontrée, associée au potentiel d'intégration tridimensionnelle, ouvre la voie au développement de dispositifs de traitement de signal à faible coût et haute performance pour les futurs systèmes de communication térahertz.

ABSTRACT

The growing demand for wireless bandwidth is pushing the exploration of the terahertz (THz) band (0.1-10 THz) as the next frontier for communications. Wavelength Division Multiplexing (WDM) is a key technology for increasing the capacity of THz systems, with integrated demultiplexers (Demux) serving as vital components. However, fabricating these devices often relies on complex, costly silicon photonics processes, hindering rapid prototyping. This thesis presents a novel, cost-effective approach to designing and fabricating high-performance THz demultiplexers using additive manufacturing (3D printing).

This approach utilizes a two-nozzle Fused Deposition Modeling (FDM) printer to fabricate suspended polypropylene circuits. We leverage the high refractive-index contrast of this design to achieve compact, low-loss guided-wave devices. The core components are Side-Coupled Waveguide Bragg Grating Filters, which were numerically optimized via finite-element modeling for the 120-165 GHz band. We successfully fabricated three distinct filters with drop channels centered at 138 GHz, 142 GHz, and 146 GHz, each exhibiting a 5 GHz bandwidth and 4 GHz inter-channel spacing.

Experimental characterization confirmed the successful demultiplexing of three channels at data rates up to 6 Gbps, with a Bit Error Rate (BER) below the forward error correction limit. The measured spectra showed strong sidelobe suppression and a broader drop port bandwidth (6 GHz) than initially modeled (4 GHz). However, transmission amplitudes were slightly lower than predicted (0.5-0.6 vs. 0.8), which we attribute to scattering losses from support structures. Furthermore, we integrated these filters into functional four-channel demultiplexers using both in-plane (horizontal) and more compact out-of-plane (vertical) configurations, interconnected via low-loss splicing.

This work establishes 3D printing as a viable and flexible platform for manufacturing complex THz integrated circuits. The demonstrated rapid prototyping capability, combined with the potential for three-dimensional integration, paves the way for the development of low-cost, high-performance signal-processing devices for future terahertz communication systems.

TABLE OF CONTENTS

LIST OF TABLES

LIST OF FIGURES

LIST OF SYMBOLS AND ACRONYMS

Acronym	Definition
2D	Two-dimensional
3D	Three-dimensional
BER	Bit error rate
CW	Continuous wave
FDM	Fused deposition modeling
FEFD	Finite element frequency domain
FFF	Fused filament fabrication
FWHM	Full width at half maximum
LNA	Low noise amplifier
OSNR	Optical signal-to-noise ratio
TEM	Transverse electromagnetic
PP	Polypropylene
SLA	Stereolithography
WBG	Waveguide Bragg grating
WDM	Wavelength Division Multiplexer

CHAPTER 1 INTRODUCTION

1.1 General Context

The rapid expansion of data-intensive technologies is driving wireless communication systems toward their fundamental bandwidth limits. Although current networks rely heavily on the already crowded microwave spectrum, this portion of the electromagnetic spectrum cannot accommodate the data rates envisioned for sixth-generation (6G) wireless systems. To meet these demands, the terahertz (THz) band (0.1–10 THz) has emerged as a leading candidate for future high-capacity wireless communication, offering exceptionally wide transmission bandwidths and enabling data rates on the order of hundreds of gigabits per second per channel.

Beyond communication, THz waves are widely used for sensing, spectroscopy, imaging, and security applications. Their unique physical characteristics—such as high spatial resolution, low photon energy, and strong material contrast—make them valuable across a broad range of scientific and industrial applications. In the communications domain specifically, THz frequencies support very high-capacity free-space links and are compatible with photonics-based transmitters and receivers.

As research advances toward practical THz communication systems, the demand for integrated, low-loss, and cost-effective THz components is growing. Traditional silicon photonics platforms offer precise, low-loss device fabrication but rely on costly cleanroom facilities and are not ideal for rapid prototyping. Recent advances in additive manufacturing provide a compelling alternative: several 3D-printing thermoplastics exhibit excellent transparency and low absorption in the THz range. This makes 3D printing a promising pathway for the rapid prototyping and fabrication of THz waveguides, couplers, resonators, and other integrated photonic components.

In this context, integrated wavelength-division multiplexing (WDM) is a powerful approach to increasing the capacity of THz links by enabling multiple frequency channels to be transmitted simultaneously. A critical element of any WDM system is the demultiplexer, which separates closely spaced spectral channels. However, designing compact, high-performance THz demultiplexers remains challenging due to fabrication limitations and the need for precise geometric control.

This thesis addresses these challenges by employing fused-filament 3D printing of polypropylene (PP), a thermoplastic with low THz absorption, to realize compact, suspended-in-air

integrated circuits that incorporate waveguides, Bragg gratings, directional couplers, and fully functional THz demultiplexers.

1.2 Challenges and objectives

The development of 3D-printed terahertz (THz) devices for communication systems presented several challenges. One of the primary issues was achieving the precision required for high-frequency THz applications. Although 3D printing offers flexibility and cost-effectiveness, it also introduces difficulties in maintaining the high accuracy needed for components such as waveguides, gratings, and couplers. Variations in nozzle speed, filament quality, and printing parameters can lead to structural deviations that negatively affect component performance. Moreover, achieving consistent quality in 3D-printed components required substantial optimization of the printing process to minimize fabrication errors, including warping and adhesion issues.

Another major challenge was selecting suitable materials for the THz circuits. Polypropylene, chosen for its high refractive-index contrast and low loss in the THz range, posed its own fabrication challenges. Maintaining the material's integrity and performance during printing required careful control of the printing environment and parameters. While advantageous for THz applications, the material's properties also demanded a cautious balance between ease of fabrication and the high precision needed in the final components. The integration of suspended elements, such as grating couplers and waveguides, added further complexity. These components require precise alignment and mechanical support to ensure proper device performance. Incorporating these subcomponents into functional systems without affecting their optical properties was a significant challenge, and the mechanical support structures had to be innovatively designed to maintain stability while avoiding interference with the device's performance.

Furthermore, the overall performance of the fabricated devices did not always match theoretical predictions. Discrepancies such as frequency shifts and lower-than-expected drop amplitudes were observed, often attributed to scattering losses from supporting structures and variations in the 3D printing process. These issues required additional testing and refinement of both the design and fabrication processes to achieve the desired performance under real-world conditions. Despite these challenges, the research sought to overcome these obstacles by refining the printing process, selecting suitable materials, and optimizing component integration, all aimed at producing high-performance 3D-printed THz circuits for communication systems.

The objectives of this research were to overcome the challenges described above and demonstrate the potential of 3D printing for the development of high-performance THz devices for communication systems. The primary goal was to fabricate integrated THz devices, such as demultiplexers and filters, using 3D printing technology, achieving low-loss, high-performance operation in the 100–200 GHz range. This required careful selection of materials, such as polypropylene, and optimization of 3D printing parameters to minimize losses and ensure precise component fabrication. Another key objective was to refine the printing process to address fabrication challenges such as warping and adhesion issues. Adjustments to parameters, including nozzle speed, filament quality, and layer alignment, were necessary to improve the consistency and accuracy of printed components, ensuring repeatable, high-quality results across multiple samples. Additionally, the research aimed to integrate individual components, such as waveguides, grating couplers, and Bragg gratings, into fully functional THz devices. Achieving this required the design of efficient mechanical support structures and the development of low-loss splicing techniques to maintain optimal performance in the final integrated devices.

The research aimed to validate theoretical predictions by experimentally testing the fabricated devices. Parameters such as insertion loss, bandwidth, and bit error rates (BER) were measured for the demultiplexers to demonstrate the viability of 3D-printed THz devices for high-speed communication systems, with a focus on achieving data rates up to 6 Gbps. Another important goal was to establish the practical application of 3D-printed THz devices in multi-channel systems. The research focused on creating 3-channel demultiplexers operating in the 100–200 GHz frequency range and capable of efficiently separating multiple frequency channels. Successfully demonstrating these devices would underscore the potential of 3D printing for scalable, low-cost manufacturing of complex THz communication components. Finally, the overarching objective was to demonstrate the potential of 3D-printed THz circuits for next-generation wireless communication systems, such as 6G. The research aimed to highlight how the low-cost, rapid-prototyping capabilities of 3D printing could enable the fast development and deployment of THz-based communication technologies, which will be crucial for meeting the growing data demands of future wireless networks.

1.3 Thesis structure

This thesis is organized as follows. Chapter 2 provides a detailed literature review on THz communications and 3D-printed photonic devices. Chapter 3 outlines the overall methodology, including the simulation, fabrication, and characterization procedures.

Chapter 4 (Article 1) presents a comprehensive study of 3D-printed demultiplexer circuits,

covering their design, fabrication, and communication characterization. Chapter 5 includes conference presentations that were published during this project, and Chapter 6 presents the technical challenges and future continuation of the project.

Finally, Chapter 7 concludes the thesis by summarizing the key findings, discussing the technical challenges encountered, and proposing directions for future research.

CHAPTER 2 LITERATURE REVIEW

In recent years, terahertz (THz) systems have seen significant advancements, driven by more powerful sources and highly sensitive detectors. These developments have expanded the range of applications, including semiconductor and high-temperature superconductor characterization, tomographic imaging, label-free genetic analysis, cellular-level imaging, and chemical and biological sensing. The THz electromagnetic spectrum, ranging from 0.1 to 10 THz (10^{12} cycles per second), lies between the infrared and microwave regions (as shown in Figure 2.1).

Unlike the neighboring bands, THz radiation faced challenges early on due to high atmospheric absorption, which limited interest and funding for THz science. Traditionally, THz spectroscopy has been used by chemists and astronomers to study the rotational and vibrational properties of simple molecules. However, over the past two decades, significant advances in materials research have led to more powerful and efficient THz sources.

This progress has broadened the applications of THz systems across various sectors, including the semiconductor, medical, manufacturing, space, and defense industries. Recent significant technical developments have increased the potential and visibility of THz systems, making terahertz technology an increasingly promising area of research [1, 11–13].

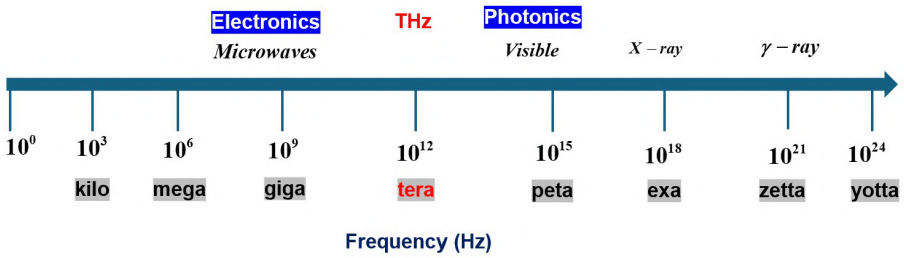

Figure 2.1 Electromagnetic spectrum [1].

The distinctive properties of THz waves, such as their non-ionizing nature, large bandwidth, strong absorption by water molecules, and high directivity, make them suitable for a wide range of applications in both fundamental and applied fields. However, some of these properties can also present challenges for specific applications. For example, the strong absorption by water molecules enables THz waves to be used effectively in label-free detection of abnormalities in biological tissues. However, it also requires precise alignment between the transmitter and receiver antennas to ensure reliability. THz waveguides and fibers provide an efficient way to manipulate THz radiation. A variety of THz waveguides have been

developed for diverse applications, including suspended-core fibers for label-free bacteria detection, dielectric pipe waveguides for sensing powders and liquid-vapor mixtures, dielectric/metamaterial/sapphire fibers for THz spectroscopy and imaging, as well as various fiber and waveguide-based functional devices for THz communication applications. As novel uses for THz waveguides and fibers continue to emerge, fabrication techniques for these components have also advanced. While the high directivity of THz waves offers significant advantages in secure communication systems, it also presents challenges for establishing stable communication links.

2.1 Terahertz Communications

The exponential growth of wireless data traffic is driving the exploration of new spectrum frontiers. Terahertz (THz) communications, which operate in the largely untapped frequency band between millimeter-waves and infrared light (0.1-10 THz), are emerging as a foundational technology for next-generation systems. This band can support the staggering data rates—from tens of gigabits per second to over a terabit per second—required for future applications. Unlike free-space optical links, which suffer from significant scattering in adverse weather, THz waves demonstrate greater resilience for outdoor use. For indoor environments, they offer an optimal balance: they are easier to manage than optical beams while providing substantially wider bandwidth than conventional radio waves [14–17].

International efforts to exploit THz technology are actively progressing. Foundational initiatives such as NASA's THz Technology Program and the European Union's WANTED project laid the groundwork early. Japan demonstrated a practical application by using a THz link for HDTV broadcasting during the 2008 Beijing Olympics. In China, a major national research initiative resulted in the country's first laboratory-scale THz system. This global engagement is further evidenced by the work of standards organizations, which are now addressing the allocation and regulation of this valuable spectral resource.

The development of practical THz systems demands innovation across multiple domains, beginning with core hardware components. Central to solid-state systems is the superheterodyne receiver, which depends on Schottky barrier diodes for frequency conversion. The progression of these diodes illustrates a clear trajectory of technological refinement: starting with delicate, manually assembled "whisker-contacted" diodes, advancing to more robust planar diodes, and culminating in the contemporary implementation of integrated planar diodes within monolithic microwave integrated circuits (MMICs), which deliver superior performance at high frequencies.

The THz modulator represents another essential component, responsible for encoding data onto the carrier wave. The advent of metamaterials—artificially structured materials capable of manipulating THz waves in novel ways—has significantly advanced this field. By integrating metamaterials with semiconductors or emerging materials such as graphene, researchers have developed high-speed modulators. Phase modulation presents particular difficulties, especially in achieving substantial and controllable phase shifts. This device enables a significant phase shift of up to 138 degrees through laser-induced dynamic control of material properties, providing a critical capability for sophisticated data-encoding schemes.

Efficient antennas are equally crucial for transmitting and receiving THz signals. Antenna design at these frequencies requires a careful balance between performance and manufacturing precision. While conventional options like horn and reflector antennas remain in use, they demand microscopic fabrication accuracy. A prominent alternative is the photoconductive antenna, which often serves as both a signal generator and a radiator. Current research is increasingly focused on developing dynamic antennas capable of electronic beam steering. These designs employ tunable materials, such as liquid crystals or graphene, to create reconfigurable metasurfaces. [18–22].

The design of reliable THz networks requires a thorough understanding of wave propagation characteristics. THz signal transmission faces severe challenges, as it is constrained not only by distance but also by molecular absorption, primarily from atmospheric water vapor. These limitations make long-range outdoor links particularly difficult, leading initial applications to focus on indoor settings. Channel modeling involves a fundamental trade-off between highly accurate but computationally intensive ray-tracing methods and less precise but more efficient statistical models. Furthermore, real-time channel estimation with large antenna arrays presents substantial difficulties, prompting the adoption of compressed sensing techniques to reduce complexity.

In this demanding propagation environment, precise energy focusing is essential rather than optional. Beamforming addresses this by employing large antenna arrays to generate narrow, high-gain beams that overcome significant path loss. A leading solution, hybrid beamforming, effectively combines analog and digital techniques to balance performance with power efficiency. Furthermore, maintaining alignment for these highly directional beams requires sophisticated tracking systems. These systems continuously adjust beam direction, often utilizing predictive algorithms and machine learning to anticipate user movement and ensure a stable connection.

These fundamental technologies have materialized in two primary system architectures. The first is the solid-state THz system, which employs frequency mixing to upconvert lower-

frequency signals. A representative example is the 220 GHz system developed by the University of Electronic Science and Technology of China (UESTC). The second architecture employs spatial direct modulation, where data is directly encoded onto a high-power THz carrier. This approach shows promise for long-distance links but remains constrained by the limited speed of current modulators.

The unique properties of terahertz (THz) waves enable transformative applications across multiple domains. Potential implementations include indoor networks capable of seamless wireless virtual reality and holographic videoconferencing, as well as secure military communications that leverage narrow, difficult-to-intercept beams. Furthermore, this technology could revolutionize data center infrastructure by replacing complex cable networks with high-speed wireless links, substantially reducing costs and power consumption. Space communications represent another promising frontier; the vacuum environment eliminates atmospheric absorption, making THz bands exceptionally suitable for satellite networks and hypersonic aircraft communications.

Despite considerable progress, several technical obstacles must be overcome before widespread THz deployment becomes feasible. Critical needs include more powerful and efficient THz sources, amplifiers, and modulators. Furthermore, the extreme bandwidth requirements outpace the capabilities of current analog-to-digital converters (ADCs), which are either unavailable or prohibitively power-intensive. This limitation is driving research into alternative architectures, such as simplified one-bit ADCs paired with sophisticated digital signal processing algorithms. Additionally, the highly directional nature of THz links necessitates a complete redesign of network protocols for fundamental operations like neighbor discovery and media access.

THz communication represents a paradigm shift in wireless technology, offering a substantial leap in capacity rather than an incremental improvement. Although significant challenges in hardware and system design persist, ongoing global research is steadily establishing the foundation for a terabit-per-second future. From the refinement of individual components to the demonstration of integrated systems, the essential pillars of a THz-connected ecosystem are progressively falling into place.

The paper review on Terahertz Communications Research by Kleine-Ostmann and Nagatsuma serves as a cornerstone in the field, articulating both the urgent need for and the initial advances in terahertz (THz) wireless communication. The authors highlight the exponential growth in wireless data traffic, which compares the capacity trends of wired and wireless technologies. This surging demand is projected to exhaust conventional radio frequencies, prompting the exploration of the lower THz range—specifically above 275 GHz—as the next

frontier. This spectrum is critical for supporting future applications that require data rates in the tens of gigabits per second, such as uncompressed ultra-high-definition television and massive data transfers in proximity-based networks.

A fundamental challenge for THz systems is the significant signal attenuation with distance. To overcome this, highly reliable components must be developed. The review provides a thorough classification of the different technological approaches for transmitters and receivers. As shown in Figure 2.2, there are three primary transmitter designs: all-electronic systems using multiplier chains and integrated circuits (ICs), photonics-based systems that rely on high-speed photodiodes, such as the Uni-Traveling-Carrier Photodiode (UTC-PD), and THz-laser-based systems, such as Quantum Cascade Lasers (QCLs).

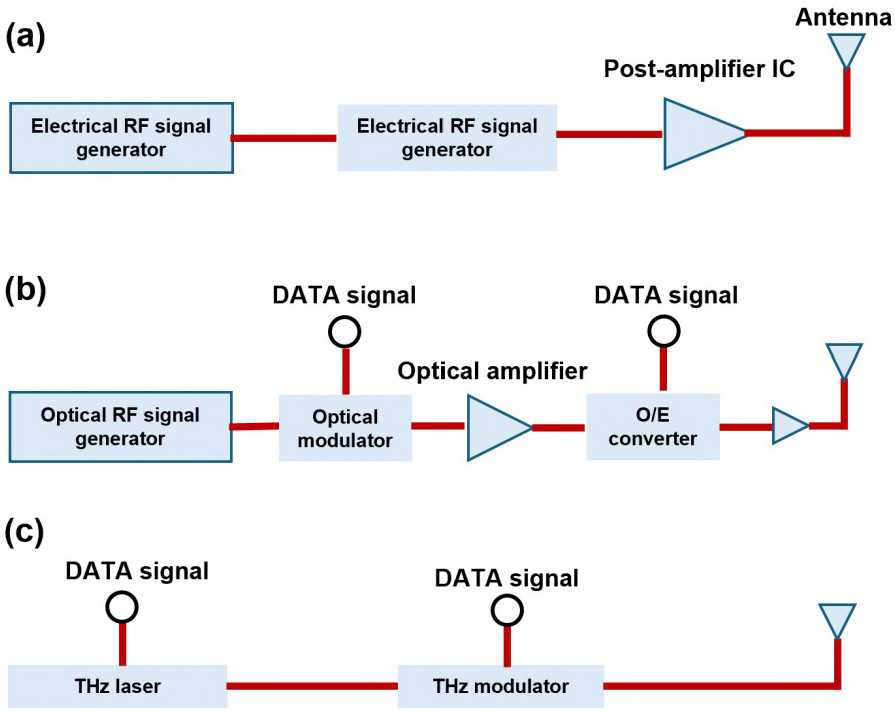

Figure 2.2 Configurations of THz transmitters and required components. a All electronics-based systems. b Photonics-based system. c THz laser-based system. Amplifier ICs of (b) and (c) are not always necessary [2].

Similarly, Figure 2.3 illustrates the receiver architectures, emphasizing the contrast between the simpler direct-detection scheme based on Schottky barrier diodes and the more sensitive heterodyne detection approach, which is indispensable for realizing high-data-rate communication links.

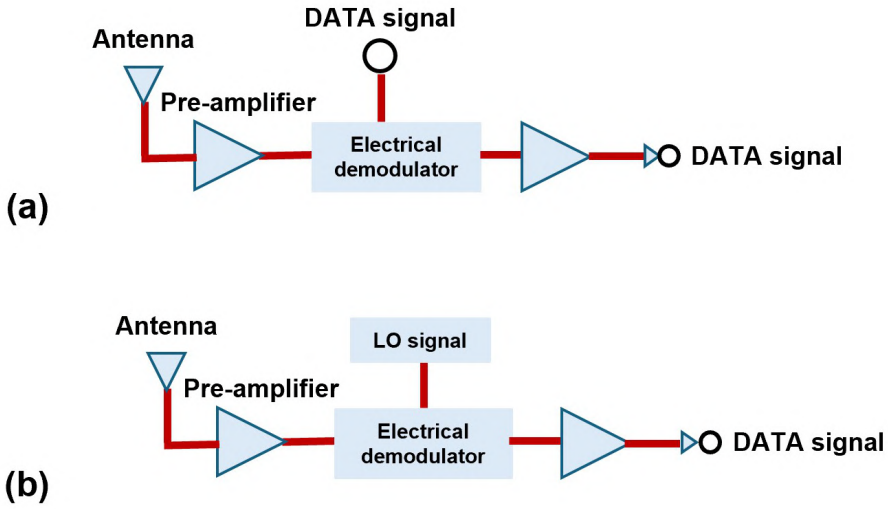

Figure 2.3 Configurations of THz receivers and required components. a Direct detection system. b Heterodyne detection system. Preamplifier ICs are not always necessary [2].

Several key developmental milestones exemplify the integration of these components into functional systems. Early implementations operating at 120 GHz achieved data rates of 10 Gbit/s over extended distances. To further enhance data throughput beyond 20 Gbit/s, subsequent research efforts advanced into the 300–400 GHz frequency band.

Figure 2.4 illustrates the block diagram of a pioneering photonics-based communication link operating within this frequency range.

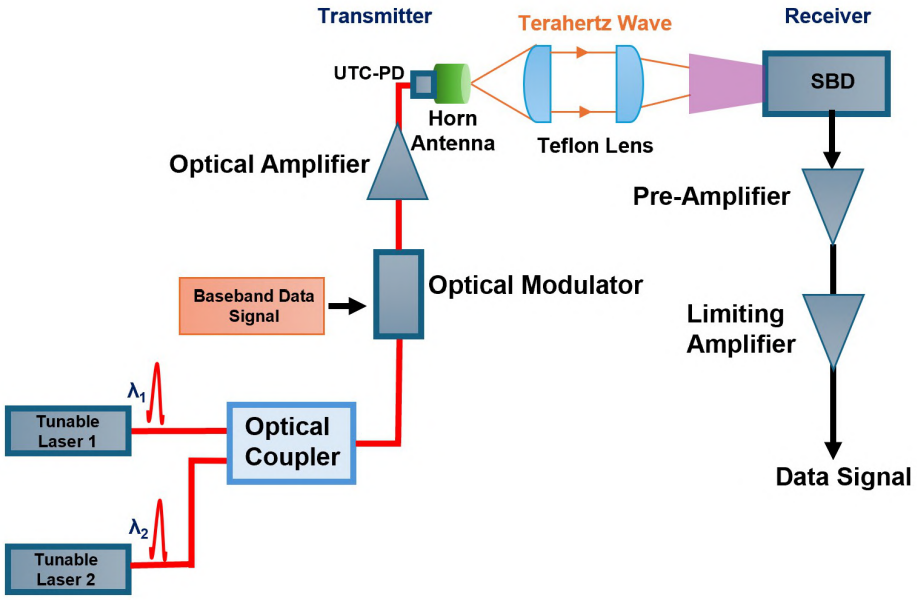

Figure 2.4 Block diagram of the wireless link using photonics-based terahertz-wave transmitter. [2].

In addition to the development of core transceivers, this review highlights several critical enabling research directions, including advanced channel modeling based on ray-tracing techniques for optimizing indoor non-line-of-sight propagation. It also introduces the innovative concept of employing omnidirectional dielectric mirrors to enhance signal coverage by strategically increasing wall reflectivity. Overall, THz communications are positioned as a pivotal enabler of ultra-high-bandwidth wireless connectivity, with future progress contingent on continued advances in semiconductor integrated-circuit technologies and the favorable resolution of international spectrum allocation policies.

2.2 Additive manufacturing (AM)

Additive manufacturing (AM), also known as 3D printing, has emerged as a transformative technology for fabricating electromagnetic (EM) components, offering unparalleled design freedom to create complex three-dimensional structures that are often impractical or prohibitively expensive to produce using traditional methods. The 3D printing technique has recently found applications in various engineering fields due to its ability to produce freeform 3D structures beyond the ability of traditional subtractive manufacturing methods. In this respect, the field of THz photonics is no exception. The adoption of 3D printing has revolutionized THz optics and device manufacturing and will continue advancing this field for

years to come [23–26]. Interest in 3D-printed optics and photonics is rapidly growing among both industry and academic researchers, driven by the unique capabilities 3D printing offers that cannot be achieved through traditional manufacturing methods. 3D printing presents tremendous opportunities for developing new integrated systems in optics and photonics. While various manufacturing approaches have been developed, no single method can simultaneously meet the demands for small features, low roughness, and high-speed production. This limitation opens up vast opportunities for innovation in 3D-printed photonics. In addition to the availability of advanced 3D printing technologies, the development of printable materials for fabricating 3D-printed optics and photonics devices is equally critical. 3D printing offers exceptional design flexibility, enabling the combination of multiple materials in a single process while facilitating the creation of complex functionalities. As an up-and-coming solution, it holds immense potential for optics and photonics applications, thanks to its ability to fabricate 3D structures with arbitrary architectures and to manufacture on non-planar surfaces. This technology significantly simplifies design processes and streamlines manufacturing workflows. By integrating materials with specific optical properties into intricate 3D structures, novel integrated systems can be developed. Additionally, different components of multi-part functional systems can be interconnected in three-dimensional space. Furthermore, 3D printing reduces material waste, making it an environmentally friendly alternative compared to traditional top-down manufacturing methods.

In recent years, additive manufacturing, in conjunction with various materials, has been extensively applied to fabricate optical and photonic devices spanning the visible spectrum to the THz and even microwave ranges. Due to resolution limitations, techniques such as fused deposition modeling (FDM), direct ink writing (DIW), and selective laser sintering (SLS) have often been employed to print larger optics and photonics devices that operate at lower frequencies on the electromagnetic spectrum, including the microwave and THz ranges. For instance, FDM printing, in combination with thermoplastic polymers, has been widely used to produce microwave and THz lenses. The PolyJet technique, which utilizes photocurable materials, is employed to create intricate 3D optical devices. DIW, using acrylates, epoxies, conjugated polymers, and conductive inks, has been used to produce light-emitting diodes (LEDs) and photonic crystals. SLS, employing powders, is used to manufacture micron-scale 3D helical structures and diffractive terahertz band lenses. For higher-resolution optical components, techniques such as stereolithography (SLA) and direct laser writing (DLW) are commonly used [3].

The extrusion-based printing technique is a cost-effective, straightforward method among 3D printing techniques. It works by continuously extruding semi-liquid materials through a nozzle, which are then selectively deposited layer by layer onto the substrate. Although

extrusion-based printing tends to be slower and lower-resolution, it can handle a broader range of viscosities and is less prone to clogging. This technique can be further classified into several types, including filament-based extrusion, plunger-based extrusion, pneumatic-based extrusion, and screw-based extrusion [3, 27, 28].

In our project, we have used Filament-Based Extrusion Printing. Fused deposition modeling (FDM), introduced by Scott Crump in the early 1990s, is a trademark of Stratasys Inc. It is also commonly known as filament-based extrusion or fused filament fabrication (FFF). Due to its low cost, simplicity, and patent expiration, FDM has become the most widely used 3D printing technology. Many low-end FFF printers are used for prototyping and non-commercial functional applications, especially among hobbyists and designers. In the FFF process, filament material is fed into the extrusion head, where it is heated to a molten state. The semi-liquefied filament is then deposited through the nozzle onto a platform to form a 2D layer. This process is repeated on top of the previous layer until the desired 3D structure is created. The filament is typically fed into the heating chamber by a roller-and-gear mechanism, where it is heated and deposited onto the build platform. The feedstock material comes in the form of a filament spool (Fig. 2.5). In FFF, polymers and thermoplastics such as poly(lactic acid) (PLA), polymethyl methacrylate (PMMA), polyethylene (PE), acrylonitrile butadiene styrene (ABS), polycarbonate (PC), polyamide (PA), polypropylene (PP), and thermoplastic polyurethane (TPU) are commonly used for fabricating optics and photonics devices. The extrusion temperature typically ranges from 200°C to 400°C, depending on the material's melting properties. To improve adhesion between adjacent layers, the target substrate is often heated to 100°C. Additionally, a dual-extruder FFF printer can be used for multi-material fabrication.

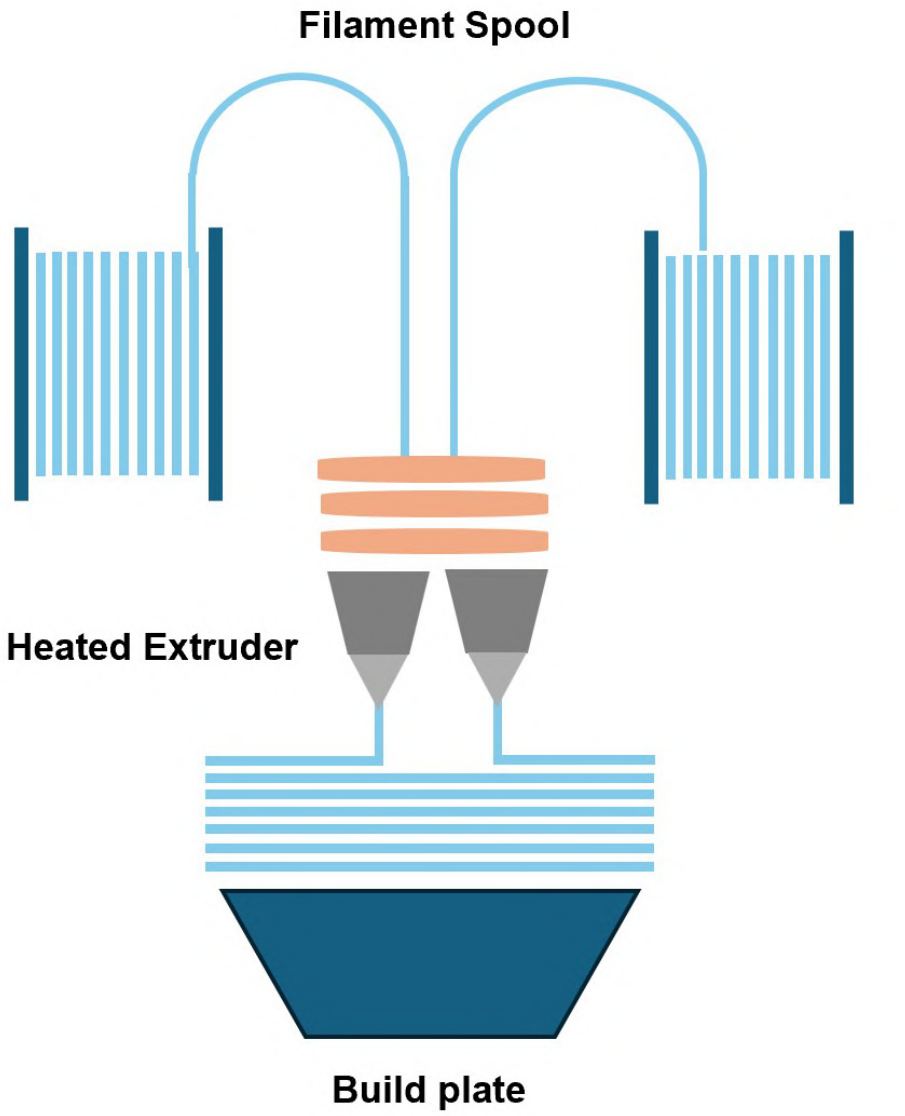

Figure 2.5 Schematic drawing of Filament-based Extrusion system [3].

The diameter of the extrusion nozzle limits the spatial resolution of FFF and typically ranges from 100 to 400 m. However, it suffers from poor resolution and inferior surface quality, which restricts its use in microwave and THz applications. Some components produced using the FFF method, such as reflective optical elements, may require post-processing. Annealing is one commonly used post-processing step that can significantly enhance the performance of optical components [3].

Several studies have demonstrated the use of FFF for fabricating 3D-printed optics and

photonics devices, including terahertz gratings [36,37], flat optics, quasi-Wollaston prisms, optical fibers, step-index optical fibers, microstructured polymer optical fibers, optical fibers with special-shaped cores [44], hollow-core waveguides [35], and lenses. The FFF printing technique is typically used to fabricate these devices directly.

The rapid development of terahertz (THz) imaging technology necessitates the creation of highly efficient optical components. Kinoform diffractive elements, such as lenses and gratings, are promising candidates for THz beam manipulation due to their smart focusing properties [29].

The two gratings differ fundamentally in their spatial period relative to the operational terahertz wavelength of 1.15 mm. The top image shows the sparse grating, characterized by a period-to-wavelength ratio of $\Lambda/\lambda = 4.16$. This significant ratio results in widely spaced, shallow triangular teeth with a low aspect ratio. In contrast, the bottom image displays the dense grating with a period-to-wavelength ratio of $\Lambda/\lambda = 1.17$. This small ratio necessitates high-aspect-ratio features, appearing as closely packed, deep teeth with steep, nearly vertical sidewalls. Additive Manufacturing (AM) is often considered the future of manufacturing due to its ability to create structures with arbitrary geometries. This capability is particularly valuable for meeting the growing demand for better and cheaper wireless devices, such as antennas and waveguides, as communication systems become ubiquitous.

2.3 Wavelength Division Multiplexing

Wavelength-division multiplexing (WDM) is a technology that combines multiple optical wavelengths for transmission over a single fiber. This scheme is conceptually equivalent to frequency-division multiplexing (FDM), as employed in microwave radio and satellite systems. A critical aspect shared by both is the necessity for sufficient spacing between the individual wavelength or frequency channels to mitigate interchannel interference [30, 31].

Multiplexing is an essential technique for increasing the capacity and efficiency of optical communication systems. By combining multiple channels of information onto a single waveguide, multiplexing allows for the transmission of large amounts of data over long distances at high speeds. WDM systems offer key advantages, including increased transmission capacity per fiber, reduced costs, the ability to carry different signal types simultaneously, and easy future expansion. The design of these systems depends heavily on the performance of optical multi/demultiplexers, along with other wavelength-sensitive components such as light sources and detectors, which are also briefly addressed.

One approach to multiplexing is wavelength-division multiplexing (WDM), which uses differ-

ent wavelengths of light to encode multiple channels. Another approach is time-division multiplexing (TDM), which uses different time slots to separate channels. However, both WDM and TDM suffer from certain limitations, including cost, complexity, and signal degradation over long distances [5,32]. Wavelength Division Multiplexing (WDM) remains a critical technique in modern optical communication systems, enabling the simultaneous transmission of multiple signals over a single optical fiber by assigning each a distinct wavelength. As data demand continues to grow, the need for compact, efficient, and scalable WDM devices has intensified.

Two recent approaches, one based on inverse design using low-index materials and the other leveraging nonlinear switching via TOAD (Terahertz Optical Asymmetric Demultiplexer)—offer promising solutions to longstanding challenges in WDM design, including polarization sensitivity, fabrication complexity, and speed limitations. The first approach, presented by Icli et al. [4], introduces a polarization-insensitive WDM device designed using an inverse-optimization framework. Unlike conventional WDM designs that rely on high-index materials and manually engineered geometries, this method uses a computational algorithm (SPINS-b) to generate a compact photonic structure that separates two wavelengths, 1.30 µm and 1.55 µm, into distinct output waveguides. Notably, the device is fabricated from polylactic acid (PLA), a low-refractive-index material with n 1.55. This choice is unconventional, as low-index materials typically suffer from weak confinement and high propagation losses. However, the inverse design algorithm compensates for these limitations by optimizing the internal geometry to maximize transmission and minimize crosstalk. Figure 2.6 shows the demultiplexing schematic of the designed PIWDM device, which separates the incoming broadband light (ranging from 1.2 to 1.6 µm) into two guided modes at specific target wavelengths: 1.30 µm, directed to the upper waveguide (WG-II), and 1.55 µm, directed to the lower waveguide (WG-I). This separation is achieved for both TE and TM polarizations. The output waveguides are positioned laterally relative to the input waveguide channel within the structure.

The resulting device is not only compact but also polarization-insensitive, functioning effectively for both transverse electric (TE) and transverse magnetic (TM) modes. This characteristic is particularly valuable in practical applications, where maintaining polarization control can be challenging. To validate the design, the authors scaled the device to operate in the microwave regime and fabricated it using 3D printing. Experimental measurements showed transmission values of 4.87 dB and 2.18 dB for TE modes, and 2.19 dB and 2.23 dB for TM modes, with low crosstalk between channels. These results confirm the feasibility of using low-index materials for high-performance WDM devices when paired with advanced design techniques. The implications of this work are significant. First, it demonstrates that

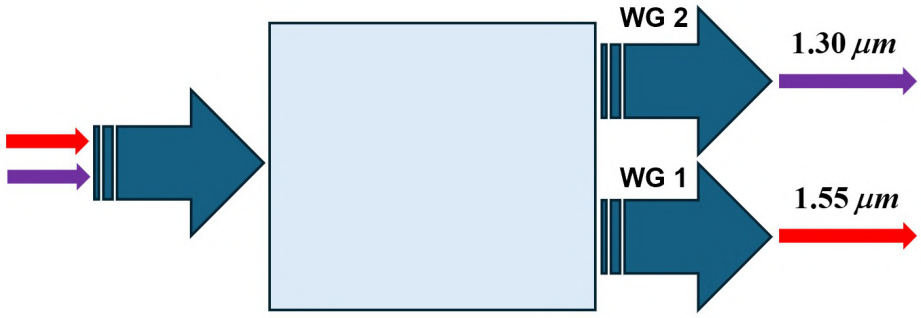

Figure 2.6 Schematic depiction of the PIWDM device [4].

low-cost, easily fabricated materials such as PLA can be used to build functional photonic components, reducing reliance on expensive cleanroom processes and high-index substrates. Second, the device's polarization-insensitive nature simplifies system integration, especially in environments where polarization fluctuations are common. Third, the use of inverse design opens new possibilities for creating non-intuitive geometries that outperform traditional designs, particularly in terms of footprint and fabrication tolerance. In contrast to the passive inverse-designed WDM device, the second work by Gayen [5] explores an active optical multiplexer architecture based on TOAD. TOAD devices operate as nonlinear switches, using the gain dynamics of Semiconductor Optical Amplifiers (SOAs) and asymmetric delay loops to control the routing of optical signals. The proposed design implements a 2:1 optical multiplexer using TOAD structures and beam combiners, allowing two input signals to be selectively transmitted based on the timing and energy of a control pulse. As shown in Fig. 2.7, the standard architecture of a TOAD-based switch incorporates two Semiconductor Optical Amplifiers (SOAs) and a delay line. The incoming optical signal is split into two paths: one passes through the delay line, while the other proceeds directly to the second SOA. The delayed signal is then combined with the direct signal within this second SOA. The SOA's nonlinear response facilitates the intended switching operation.

The core mechanism of TOAD relies on modulating the SOA gain with a control pulse, creating a temporal window during which one signal is amplified while the other is suppressed. This enables logic-level switching without electronic conversion, making TOAD-based devices suitable for ultrafast optical networks. The simulation results presented in the paper show that the multiplexer can operate at bit rates up to 20 Gbps, with high Q-factor and low bit-error rates when parameters such as control-pulse energy, SOA gain, and loop asymmetry are carefully tuned. One of the key advantages of the TOAD-based approach is its ability to

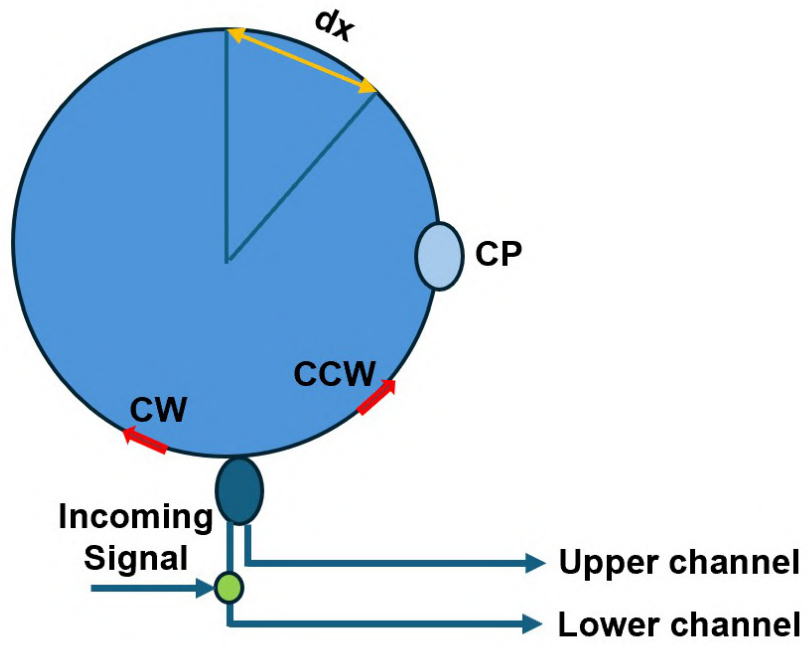

Figure 2.7 Schematic of a TOAD-based optical switch utilizing a single control pulse [5].

perform all-optical switching, eliminating the latency and bandwidth limitations of electronic processing. This makes it particularly attractive for applications in optical computing, signal processing, and high-speed data routing. However, the architecture also introduces complexity in terms of synchronization and power management. Precise timing of the control pulse is essential for correct operation, and the SOAs must be carefully managed to avoid thermal noise and gain saturation. In conclusion, the future of WDM lies in integrating passive and active components, leveraging the strengths of each to build scalable, efficient, and adaptable optical networks. The work by Icli et al. and Gayen exemplifies this duality, offering complementary solutions to the challenges of wavelength multiplexing. As research continues to explore new materials, design algorithms, and switching mechanisms, the boundaries of what is possible in optical communication will continue to expand, paving the way for faster, more innovative, and more resilient networks.

Gerd Keiser provides a comprehensive overview of Wavelength-Division Multiplexing (WDM) technology, highlighting its evolution from a conceptual idea to a fundamental component of modern telecommunications networks [6]. The rapid exhaustion of capacity in long-haul fiber networks during the 1990s served as the primary catalyst for the adoption of WDM.

Given that laying new fiber-optic cables is expensive and time-consuming, WDM emerged as the most cost-effective solution. It enables a significant increase in the capacity of a single optical fiber by allowing it to carry multiple independent data channels simultaneously, each operating on a distinct wavelength. This concept is similar to frequency-division multiplexing but is applied within the vast bandwidth of an optical fiber, particularly in the low-loss 1550-nm window.

A typical point-to-point WDM system, as depicted in Figure 2.8, comprises several key components. At the transmitting end, multiple independent light sources, such as distributed-feedback (DFB) lasers, emit signals at uniquely assigned wavelengths. These optical signals are then combined using a multiplexer, allowing them to travel through a single fiber. Upon reaching the receiving end, a demultiplexer separates the individual wavelengths, directing each one to its corresponding photodetector for signal processing. The development of efficient, cost-effective versions of these components was crucial to the commercial success of WDM.

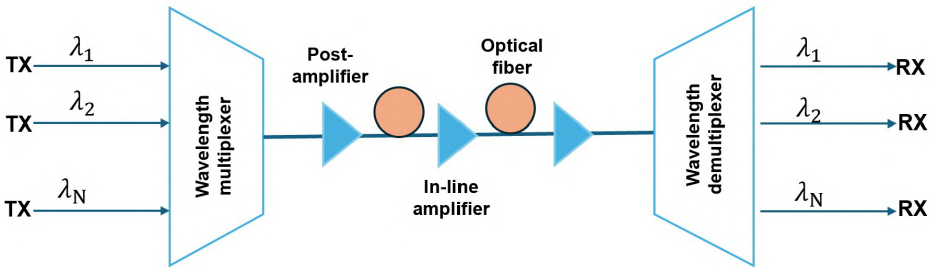

Figure 2.8 Implementation of a typical WDM link [6].

The technological core of this work focuses on a detailed discussion of the components that enable WDM. Passive devices, which function without external control, form the basic infrastructure of WDM systems. A key example is the star coupler, shown in Figure 2.9, which evenly distributes optical power from multiple input fibers to multiple output fibers. However, more advanced wavelength-selective devices are required for efficient WDM operation.

A particularly effective demultiplexing device is the Fiber Bragg Grating (FBG), used in combination with an optical circulator, as illustrated in Figure 2.10. In this setup, a multi-wavelength signal enters the circulator and is directed to the FBG, which reflects a specific wavelength (e.g.,) while passing all others. The reflected wavelength is then routed by the circulator to a separate drop port, effectively isolating it from the rest of the signal. In addition to these passive components, active devices introduce dynamic reconfigurability and enhanced functionality to WDM networks. Tunable optical filters and lasers enable

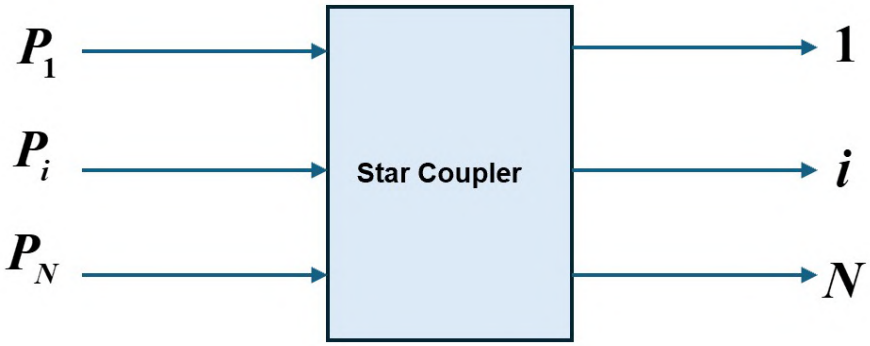

Figure 2.9 Basic star-coupler concept [6].

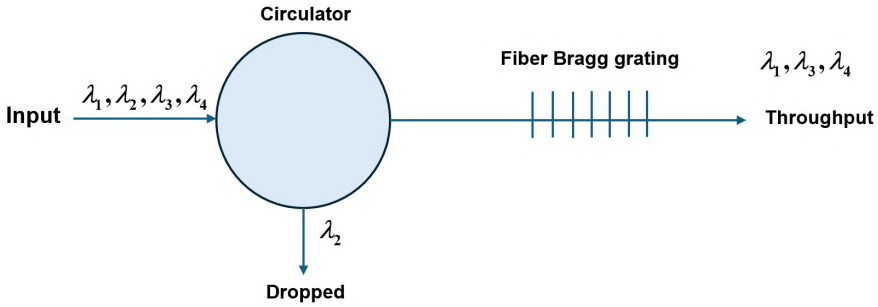

Figure 2.10 schematic of demultiplexing function using a fiber grating and a circulator [6].

network operators to select and assign wavelengths electronically, offering significant flexibility. One of the most revolutionary technologies enabling WDM's widespread use is the Erbium-Doped Fiber Amplifier (EDFA). The EDFA boosts the power of all WDM channels within its gain band simultaneously, without the need for optical-to-electrical conversion, thus enabling practical long-haul, multi-span transmission [33–37]. For the development of complex, reconfigurable optical networks, advanced components such as tunable multigrating filters are indispensable. As shown in Figure 2.11, this device uses a series of tunable FBGs positioned between two circulators to dynamically add and drop specific wavelengths from a central data trunk. This functionality is the foundation of reconfigurable optical add-drop multiplexers (ROADMs) in modern optical networks.

Designing WDM systems requires careful consideration of several operational characteristics and inherent limitations. The total system capacity is simply the sum of the bit rates of all the wavelength channels. However, this capacity is constrained by physical impairments.

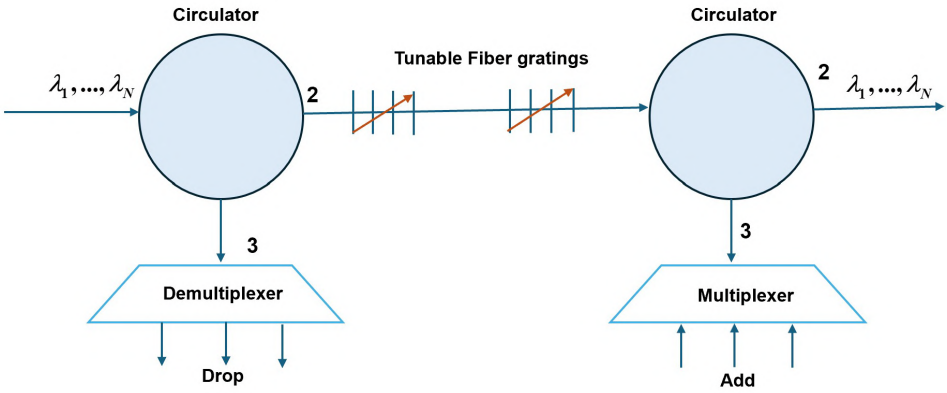

Figure 2.11 Tunable multigrating filters used to add and drop any number of N different wavelengths [6].

As the number of channels increases and their spacing narrows, crosstalk—both interchannel (between adjacent wavelengths) and intrachannel (from component imperfections)—becomes a critical issue, imposing power penalties on the system. Additionally, the accumulation of Amplified Spontaneous Emission (ASE) noise from a series of EDFAs degrades the optical signal-to-noise ratio (OSNR) over long distances. Nonlinear optical effects within the fiber, such as Four-Wave Mixing (FWM) and Stimulated Brillouin Scattering (SBS), generate additional crosstalk and distortion, particularly at high optical power levels. These challenges are mitigated through careful system design, which includes dispersion management and power control.

2.4 Fiber Bragg Grating

Fiber Bragg Grating (FBG) is a fundamental optical component inscribed within the core of an optical fiber. It acts as a highly selective wavelength-specific mirror or filter. The discovery of photosensitivity in optical fibers by Ken Hill in 1978, in which intense laser radiation could induce a permanent periodic change in the fiber core's refractive index, paved the way for the development of FBGs. The core principle of an FBG is based on the Bragg condition [7]. The grating structure, with a periodic refractive index modulation, reflects a very narrow band of light centered at the Bragg Wavelength (λ_B). All other wavelengths are transmitted through the grating with minimal loss, as shown in Figure 2.12.

The Bragg wavelength is given by:

$$\lambda_B = 2n_{\text{eff}}\Lambda \tag{2.1}$$

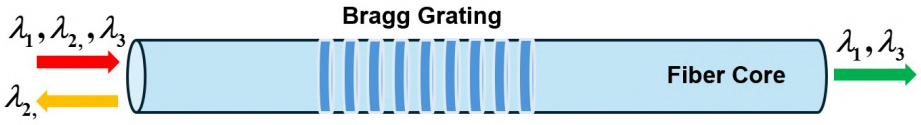

Figure 2.12 Schematic of the fiber Bragg gratings [7].

where:

- λ_B is the Bragg wavelength (reflected),
- n_{eff} is the effective refractive index of the fiber core,
- Λ is the grating period (the physical spacing between index modulations).

This equation shows that any physical parameter that alters n_{eff} (e.g., temperature via the thermo-optic effect) or Λ (e.g., strain via physical elongation or compression) will cause a shift in λ_B. This shift is the fundamental mechanism behind FBG's sensing capabilities.

The maximum reflectivity at the Bragg wavelength.

$$R_{\max} = (\tanh(\kappa L))^2 \tag{2.2}$$

where κ is the AC coupling coefficient and L is the grating length. A stronger grating (a higher κ or a longer L) leads to higher reflectivity.

For filtering applications in plasmonic circuits, waveguide-integrated Bragg gratings have been successfully demonstrated. An example of such a device, fabricated using nanoimprint lithography for mass production viability, consists of a V-groove waveguide with a built-in Bragg grating, which selectively reflects a specific wavelength band, as evidenced by the transmission dip in its spectrum.

CHAPTER 3 METHODOLOGY

In this chapter, we outline the main methodologies used in this thesis. First, we introduce the numerical simulations conducted for the theoretical development and analysis of the proposed or fabricated demultiplexers. Next, we describe the fabrication techniques used to fabricate demultiplexers. Then, we explain the two experimental systems employed for demultiplexer characterization. Finally, we detail the annealing process applied to enhance the quality of FDM 3D-printed demultiplexers.

The project introduces a groundbreaking approach to fabricating demultiplexer circuits for terahertz (THz) communications using 3D printing technology. This technique incorporates suspended-in-air grating couplers and leverages a high-refractive-index-contrast material combination specifically, polypropylene (PP) filaments suspended in air. This unique combination is highly beneficial because it minimizes losses due to absorption in the THz frequency range, a critical component in high-speed communication technologies, especially for future applications like 6G wireless networks. The key innovation here is the use of 3D printing, particularly Fused Deposition Modeling (FDM), to print integrated THz components. Unlike traditional methods, which typically rely on complex and expensive photonic crystal-based fabrication techniques or metamaterial designs that require high precision, 3D printing offers a much more accessible and cost-effective alternative. This approach allows for rapid prototyping and development of THz components without the need for costly infrastructure, providing a distinct advantage for researchers and engineers in the field. In terms of fabrication, the 3D printing process is used to print waveguides, couplers, and fiber Bragg gratings. The larger filament (800 µm) is used to print the waveguides and couplers, while the smaller filament (400 µm) is used for the fiber Bragg gratings, which are essential for achieving high-quality frequency filtering. These grating couplers, when suspended in air, enable a compact and low-loss design, crucial for maintaining the integrity of THz signals. The key advantage here is the high refractive index contrast between polypropylene and air, which results in low absorption losses and better efficiency in the THz range compared to conventional materials used in photonic devices. This method eliminates the need for the precise photonic crystal alignment and lithographic steps that are typically required in more traditional methods. This makes it simpler and more efficient to produce high-performance THz components, leading to faster turnaround times in prototyping and less expensive manufacturing processes. This, in turn, lowers the barriers to entry for THz technology and accelerates the pace of innovation in the field. Additionally, the paper highlights the challenges introduced by the 3D printing process, such as warping, adhesion difficulties, and

variations in nozzle speed or filament quality. However, the authors have addressed these issues by carefully optimizing the printing parameters to minimize deviations in the structure and enhance the overall performance of the devices. The use of mechanical supports during the printing process further aids in maintaining the stability of the suspended-in-air components, ensuring that the printed devices maintain their integrity and functionality. The experimental demonstration of the 3-channel demultiplexer, operating in the 120-165 GHz frequency range, shows promising results. These demultiplexers were tested with data rates of up to 6 Gbps and achieved bit error rates (BER) below the acceptable limits, confirming their suitability for practical communication systems. The drop port bandwidths in the experiments were measured to be broader (around 6 GHz) compared to the theoretical predictions (4 GHz), showing that the devices perform better than expected in some aspects. Additionally, sidelobe suppression was strong, which is important for ensuring that the demultiplexers can accurately separate different frequency channels with minimal interference. The 3D-printed demultiplexer also demonstrated successful integration of multiple filters, both in series (sequence) and parallel, further enhancing the system's ability to handle multiple channels. This flexibility in design allows for the creation of more complex and scalable systems for high-frequency communication, such as future THz communication networks that require high data rates and low latency. In terms of scalability, the approach allows for the integration of multiple devices within a single system, making it easier to build larger, more complex THz systems. The ease of manufacturing and the reduced cost of production means that the technology is well-suited for rapid development cycles and large-scale deployment in applications like 6G, where demand for high-speed, high-capacity communication systems will increase dramatically.

In conclusion, the 3D-printed demultiplexer circuits using suspended-in-air grating couplers represent a major advancement in THz communication technology. They combine the advantages of 3D printing—cost-effectiveness, flexibility, and scalability with high-performance optical design, offering a significant improvement over existing technologies. These devices enable the development of low-loss, high-efficiency THz components that are essential for the next generation of wireless communication systems, particularly as the demand for terabit-per-second data rates and advanced multiplexing techniques increases in 6G networks.

3.1 Numerical simulations

In this thesis, the theoretical optimization and numerical analysis of the proposed terahertz (THz) demultiplexers were conducted using the Finite Element Frequency Domain (FEFD) module within the commercial software COMSOL Multiphysics. The simulations focused on

calculating and optimizing the performance of the Through and Drop channels for demultiplexers with uniform cross-sections.

A schematic of the demultiplexer structure investigated in this work is presented in Figure 3.1. The model geometry was constructed in COMSOL, and appropriate boundary conditions were applied to simulate the propagation of electromagnetic waves and the extraction of specific frequency channels at the output ports.

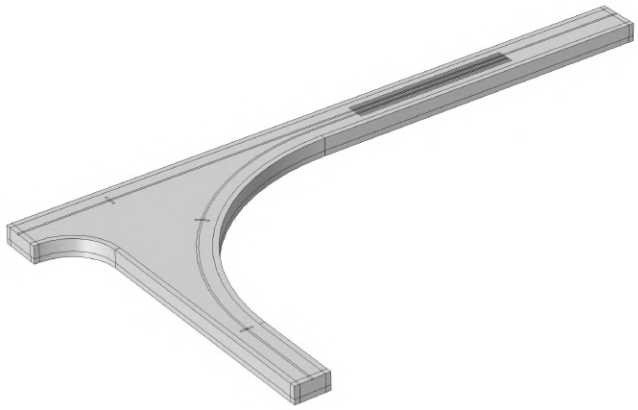

Figure 3.1 Schematic of the demultiplexer structure.

3.2 The fabrication of THz demultiplexers using FDM 3D printers

The standard printer (Raise3D Pro2) FDM-based 3D printing techniques were employed for THz demultiplexers fabrication. As illustrated in Fig. 3.2, in standard printers, the nozzle axis is aligned parallel to the printer's Z-axis, allowing models to be fabricated vertically, layer by layer.

Due to the limited build volume of standard printers, long (meter-scale) fibers must be assembled by mechanically joining shorter fiber segments with connectors. Additionally, support structures are often necessary to maintain the stability of tall, slender prints. It is important to note that, to achieve optimal optical performance of the printed demultiplexers or optical components, careful optimization of printing parameters is essential, regardless of whether post-processing techniques

3.2.1 Fused Deposition Modeling (FDM)

Fused Deposition Modeling (FDM) is an additive manufacturing technique in which objects are built layer by layer by extruding melted thermoplastic material along a predefined path.

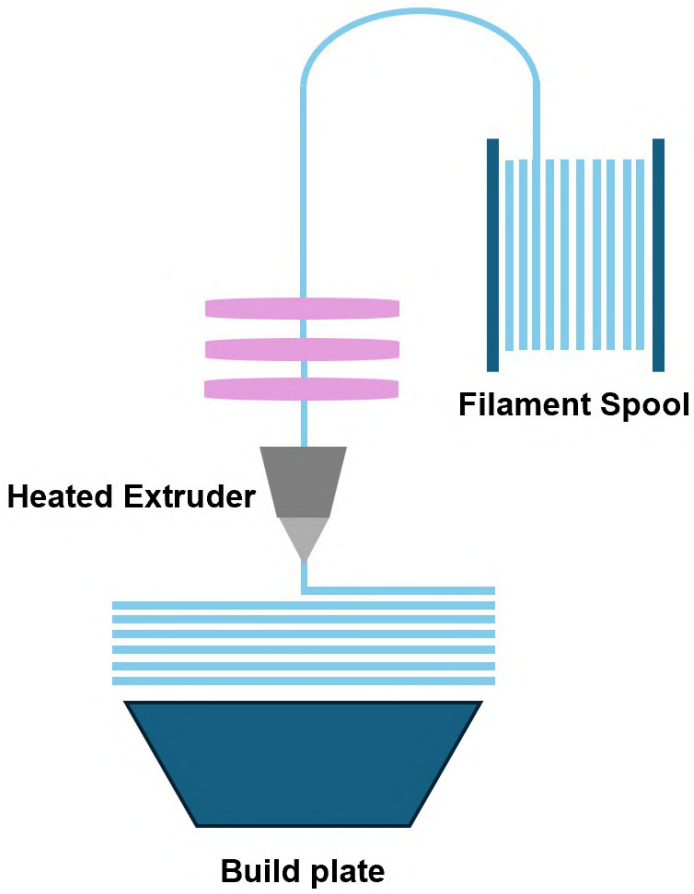

Figure 3.2 A diagram of Layer-by-Layer FDM printing.

The process begins with a computer program that slices the 3D model into hundreds of thin layers. The sliced file is then sent to the printer, which heats a metal nozzle to the required temperature. A filament of thermoplastic is fed into the heated nozzle by a gear system. The nozzle moves horizontally, guided by two belts, and deposits the melted filament onto a build platform, following the pattern of each sliced layer. After each layer is deposited, the platform lowers slightly, allowing the next layer to be printed on top. This process repeats until the full model is completed. Depending on the object's size and resolution, the printing time can range from 30 minutes to several days. On average, prints in the Fabrication Farm take about three hours to complete. Next, we present and discuss the multiparameter optimization of the 3D printing process. The FDM technique inherently introduces surface roughness with feature sizes comparable to the deposited layer thickness. Additionally, when printing fiber bulk regions at a 100% infill rate, unintentional air entrapment may occur. Both surface roughness and air pockets in the bulk contribute to additional scattering losses. However, in the low THz frequency range—most relevant for communication applications, the typical

wavelength is around 1 mm, while the layer thickness and transverse resolution of FDM printers are approximately 0.1 mm. As a result, both surface and bulk imperfections are subwavelength, and scattering from these defects follows Rayleigh's law. Our experiments employed the Raise3D Pro3 FDM printer, as shown in fig. 3.3, known for its high positional accuracy (1 µm in the XY plane and 10 µm along the Z-axis). A 1.75 mm natural transparent polypropylene (PP) filament was selected due to its high transparency and low absorption in the THz range . A standard 'Rectilinear' infill pattern was used during optimization, as it generally results in mechanically isotropic structures within the build plane. The optimal extrusion temperature for polypropylene is reported to be in the range of 190-250 °C ; in our experiments, we selected 240 °C based on the filament manufacturer's recommendation.

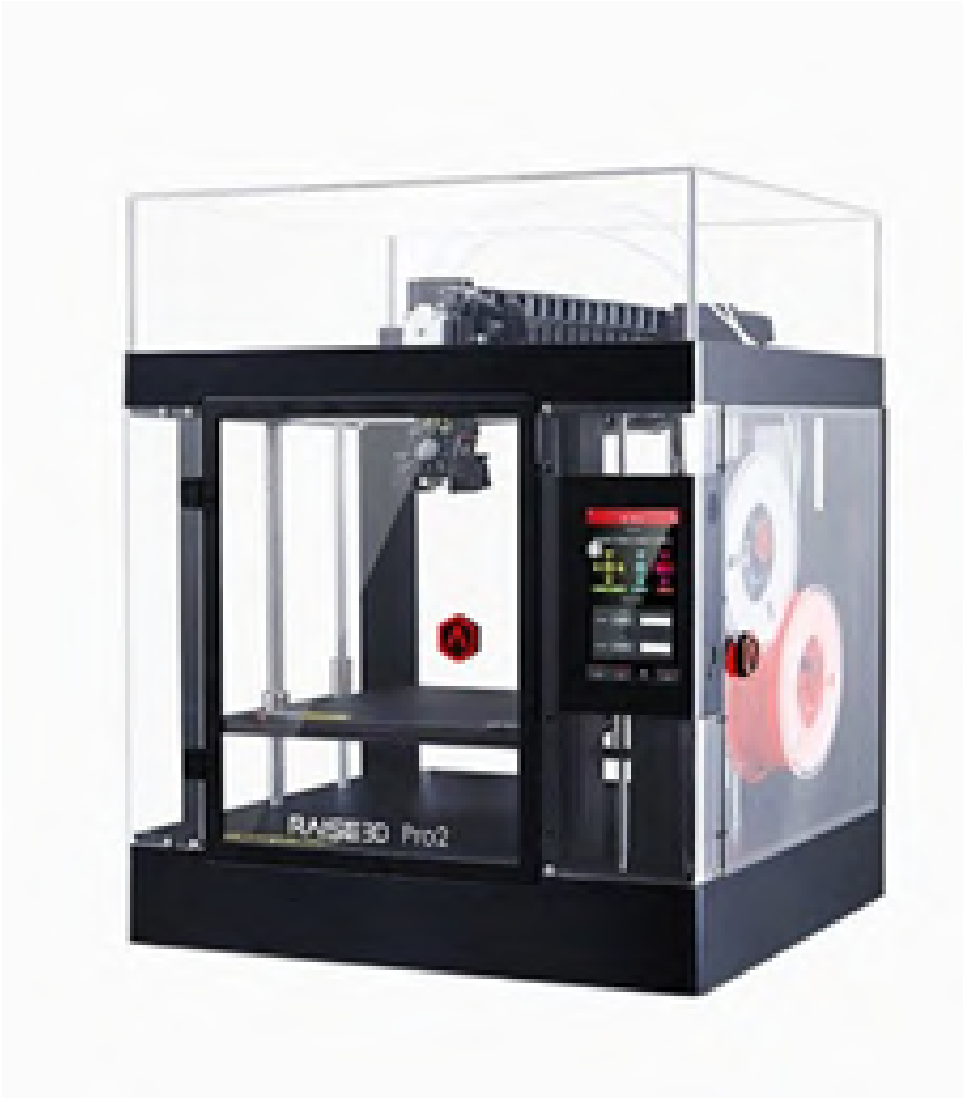

Figure 3.3 Raise3D Pro2 FDM printer [8].

The Raise3D Pro3 offers a generous build volume of 12 × 12 × 11.8 inches, enabling the fabrication of significantly larger models. Its fully enclosed design ensures stable internal temperatures, making it well suited for printing with ABS and other temperature-sensitive materials. In addition, the Pro3 is equipped with an upgraded cooling fan featuring a HEPA filter. This fan can be adjusted to control cooling intensity and effectively captures over 90% of airborne particles, helping to maintain a cleaner and safer working environment by reducing dust and emissions.

3.3 Continuous Wave THz spectroscopy system

The optical characteristics of the THz demultiplexers introduced in this thesis were examined using a Continuous Wave THz spectroscopy system, previously described in our earlier publication [38]. A schematic of the setup is shown in Fig. 3.4 and can be summarized as follows: Two tunable TeraBeam lasers, operating at carefully offset wavelengths, are employed to drive the THz photomixer (emitter), enabling the generation of THz waves through difference-frequency techniques. The emitted THz radiation, produced by the photomixer (Model: IOD-PMD-14001 from NTT Electronics Inc.), is transmitted through a WR-6 rectangular waveguide flange, which is directly aligned with the fiber under investigation. On the detection side, a horn antenna with a diameter of 10.8 mm captures the THz signal. This signal is then processed by a zero-bias Schottky detector (Model: WR8.0 ZBD-F from Virginia Diodes Inc.), which demodulates the incoming waves. To ensure signal integrity and facilitate further analysis, a high-gain, low-noise amplifier (Model: SLNA-030-32-30-SMA from Fairview Microwave Inc.) is used to boost the detected signal.

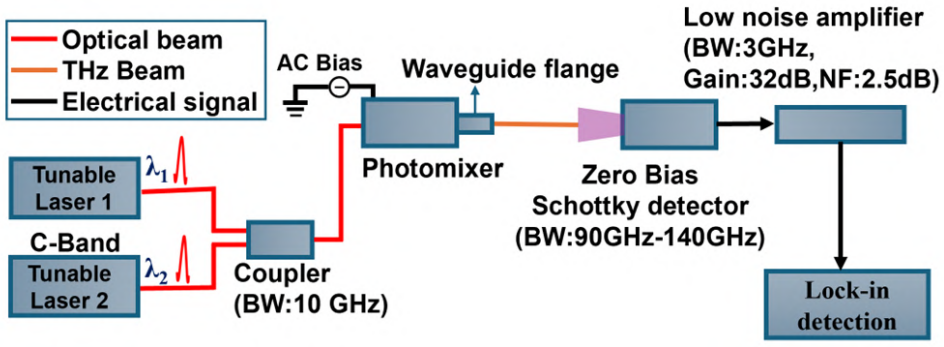

Figure 3.4 Schematic of the Continuous Wave THz spectroscopy system.

3.4 Photonics-based THz communication system

The communication performance of the THz demultiplexers presented in this thesis was assessed by measuring the Bit Error Rate (BER) of signals transmitted through the fiber at various bit rates and carrier frequencies. This evaluation was conducted using a custom-built photonics-based THz communication system, previously described in [38]. A schematic of the system is shown in Fig. 3.5 and can be outlined as follows: On the transmission side, the combined infrared optical signal from the coupler is modulated via an external electro-optic modulator (Models: LN81S-FC and MX10A from Thorlabs, Inc.). The modulation is driven by a non-return-to-zero pseudo-random bit sequence (PRBS) with a pattern length of $2^{31}-1$, serving as the baseband signal. This PRBS data, with a fixed peak-to-peak amplitude, is first connected to the modulator driver, where it is amplified before being fed into the electro-optic modulator. The resulting modulated optical signal, maintained at a constant output power, is further boosted using an Erbium-Doped Fiber Amplifier (EDFA). On the receiving end, a Bias-Tee is employed to remove the DC component from the demodulated baseband signal, followed by a low-noise amplifier (LNA) to enhance the signal strength. The final signal is then analyzed using a high-speed oscilloscope and a BER tester (Model: MP2100B from Anritsu Corporation). The target BER for this study was set to 10-12, representing an error-free transmission. The duration of each measurement, which is inversely proportional to the bit rate, was calculated using the expression [1 / target BER . bit rate]. BER measurements were performed by varying the bit rate from 1 Gbps to 6 Gbps, or by adjusting the carrier frequency at a fixed bit rate. For each configuration, the decision threshold was carefully optimized to balance insertion errors (where a digital zero is misinterpreted as one) and omission errors (where a digital one is misread as zero), thereby minimizing the overall BER.

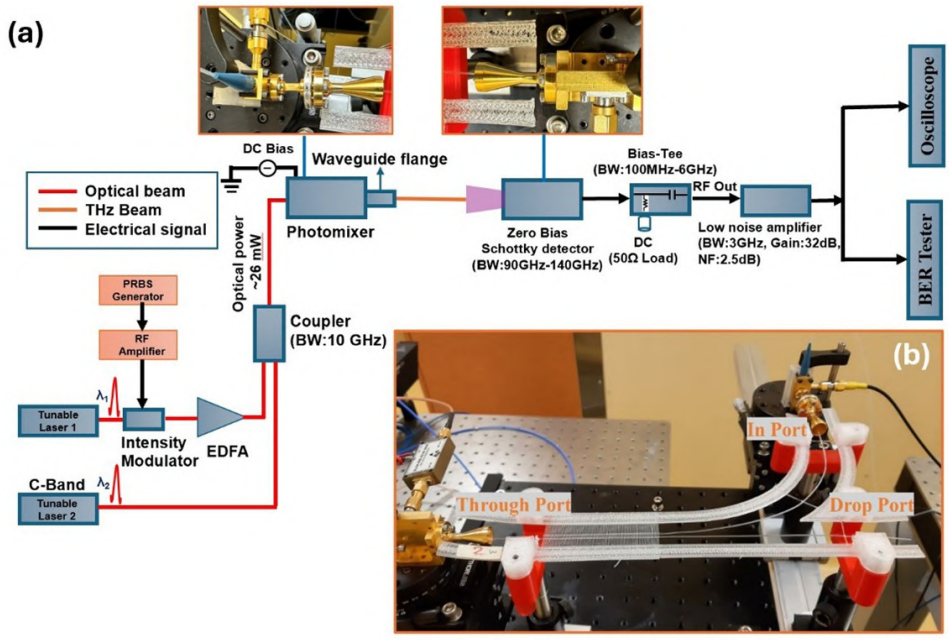

Figure 3.5 Schematic of the photonics-based THz communication system.

CHAPTER 4 ARTICLE 1: 3D-PRINTED DEMULTIPLEXER CIRCUITS USING SUSPENDED-IN-AIR GRATING COUPLERS FOR TERAHERTZ COMMUNICATIONS

This chapter addresses the issue of the 3D printed THz demultiplexers. It is a transcription of a manuscript published in IEEE Access [38]. The article was published on May 16, 2025.

4.1 Authors

Babak Yahyapour[1], Frédéric Marcotte[2], Roya Gachiloo1[1] and Maksim Skorobogatiy[1]

[1] Department of Engineering Physics, École Polytechnique de Montréal, Montreal, QC H3T 1J4, Canada.

[2]Department of Electrical Engineering, Université Laval, Quebec City, QC G1V 0A6, Canada.

4.2 Abstract

Integrated photonic circuits are in great demand for the upcoming THz communications. This work explores 3D printing to realize high-quality, high-refractive-index-contrast integrated components and devices for demultiplexing terahertz channels within the Wavelength Division Multiplexing modality. Namely, by printing integrated circuits using Polypropylene filaments suspended in air, we profit from the high-refractive index contrast of such a material combination to realize relatively compact low-loss waveguides, bends, couplers, and fiber Bragg gratings. The two-nozzle FDM printer allows simultaneous printing with filaments of two distinct sizes of 800um and 400um, with the larger filament used to make waveguides and couplers, and the smaller one used to define high-quality fiber Bragg gratings containing as much as 100 periods and featuring stop bands as wide as 10 GHz. Furthermore, by employing judiciously designed mechanical supports we show how to integrate such subcomponents into functional components such as single-channel drop filters. Finally, we developed a low-loss splicing technique for joining several components into functional devices and demonstrated four-channel THz WDM demultiplexers with in-plane (horizontal) and a more compact out-of-plane (vertical) integration. Experimentally, three-channel demultiplexers of THz signals with individual data rates up to 6 Gbps were demonstrated. Using finite element numerical modeling, integrated circuits were optimized for operation in the 120-165 GHz frequency band featuring 5 GHz individual channel bandwidths and 3 GHz inter-channel spectral spacing, and good agreement with the experiments was observed. Additionally, the measured spectra

closely resemble the simulated ones but exhibit a frequency shift of several GHz towards higher frequencies. Experimental results further reveal strong sidelobe suppression and a broader Drop port bandwidth (6 GHz vs. 4 GHz predicted). However, the measured Drop amplitudes (0.5–0.6) are lower than the theoretical predictions (0.8) due to 10% scattering losses per supporting structure. We believe that the suspended-in-air integrated terahertz circuits hold strong potential for developing various linear optic transformers that will play a key role in energy-efficient analog processing of data streams for the upcoming terahertz communications. This is because of the high quality of the resultant circuits, ease of fabrication, and low infrastructure costs necessary for their manufacturing, thus allowing low-cost fast turnaround prototyping and development of terahertz signal processing devices even with the simplest 3D printing systems.

4.3 Introduction

Most wireless systems currently operate in the overcrowded microwave band, which is insufficient to meet the future bandwidth demand. Shifting the carrier wave to higher frequencies is essential to accommodate the anticipated surge in data [19, 39]. Consequently, the terahertz (THz) frequency band (0.1-10 THz) is regarded as the next frontier for wireless communication systems [2, 40–42]. Terahertz (THz) waves situated between microwave and infrared spectral bands attracted much interest for a variety of industrial applications in sensing [43, 44], imaging [45, 46], and security [47, 48] due to their many unique properties. Specifically for communications [2, 40, 49–55], THz waves enable larger bandwidths than microwaves, potentially enabling several 100 Gbps data rates per channel without any multiplexing. The expected increase in data traffic over the next decade, driven by nascent technologies such as the Internet of Things, Virtual and Augmented Reality, Artificial Intelligence, Big Data, etc. has prompted the development of the sixth generation (6G) wireless networks that greatly surpass existing 4G and 5G network standards.

Terahertz communications is a promising technology for the 6G networks capable of terabit-per-second wireless and fiber-assisted transmission for various data-demanding applications [56–62] . To date, several demonstrations of free-space ultra-high bit rate data transfer (>100 Gbps) employed single-channel THz links with optical multiplexing [63–65], as well as advanced modulation techniques including quadrature amplitude modulation and quadrature phase-shift keying [66–68]. One promising way of data multiplexing in the THz range is Frequency Division Multiplexing (FDM), which encodes different channels using distinct carrier frequencies [5, 69]. A multiplexer (Mux) and a demultiplexer (Demux) are essential components in FDM technology. The multiplexer combines light from spatially separated spectrally

distinct sources into a single data stream, while the demultiplexer spatially separates the multiplexed frequencies into single carrier frequency channels [70–73]. The fabrication of THz devices often involves significant complexity. A standard way uses the methods and infrastructure of silicon photonics to fabricate low-loss THz optical elements [74–77]. While scalable for mass production, this approach requires access to very expensive infrastructure and entails high running costs, which makes it ill-suitable for rapid prototyping. Alternatively, certain thermoplastics used in additive manufacturing exhibit transparency to terahertz (THz) radiation, which opens an interesting opportunity for 3D printing as a cost-efficient alternative for rapid prototyping of THz devices. As a result, 3D printing has recently gained considerable attention within the Terahertz research community, leading to the development of numerous 3D-printed THz components such as freeform microwave waveguides, antennas, and basic optical elements [23, 78–83]. Furthermore, 3D printing opens a way for high-density integration of photonic circuits in three dimensions, a feat challenging to accomplish with other methods. For example, M. Ortiz-Martinez et al. developed a 3D-printed filter made of polystyrene (PS) for the sub-THz 200-300 GHz band [84]. Weidenbach et al. demonstrated 3D-printed waveguide designs, including low-loss splitters and couplers, operating at 120 GHz, fabricated from polystyrene [85]. Additionally, 3D-printed terahertz grating couplers have been designed and characterized at 120 GHz for outcoupling and focusing THz radiation [86]. Furthermore, low-loss, low-dispersion waveguides printed from PS have achieved error-free performance at a data rate of 1 Gb/s [87] . Compared to recent studies, our work presents a novel 3D-printed terahertz demultiplexer featuring suspended-in-air grating couplers, offering significant advantages in fabrication flexibility, cost-effectiveness, and scalability. Unlike the photonic crystal-based demultiplexers proposed by Li et al. [88], which rely on cascaded directional coupling waveguides created by selectively removing rows of silicon rods, our approach eliminates the need for complex lithographic fabrication and precise photonic crystal alignment. Furthermore, while Wu et al. [89] demonstrated a metamaterial-based demultiplexer with high isolation and low insertion loss, its resonance-dependent design requires high precision fabrication and limits both scalability and tunability. In contrast, our 3D-printed demultiplexer circuits allow for customized integration into various THz systems, providing a more adaptable and practical solution for terahertz communication applications. Our presented demultiplexer enables precise, wavelength-specific separation of THz signals while offering significant advantages in terms of fabrication flexibility, cost-effectiveness, and scalability. Our method leverages the versatility of even the basic FDM 3D printing to create complex geometries that are difficult to achieve with conventional techniques, ultimately enhancing signal separation and overall system performance. In this work, we demonstrate experimentally 3-channel demultiplexers with 2D (in-plane) and 3D (out-of-plane) integration

for Frequency Division Multiplexing in the 100-200 GHz spectral band using Side-Coupled Waveguide Bragg Grating Filters as enabling building blocks. The devices were fabricated from a low-loss Polypropylene dielectric using Fused Filament Fabrication (Raise 3D Pro2 series). To the best of our knowledge, this is the first time that devices of such complexity have been realized using 3D printing, in the planar and vertically integrated variants. The advanced optical performance of our demultiplexers stems from the use of polypropylene (PP) polymer in air- a high refractive index contrast material combination that offers one of the lowest absorption losses in the THz regime. However, the 3D printing process introduces several challenges, including warping, adhesion difficulties, and variations in nozzle speed, printed waveguide size, and filament quality, all of which can affect the precision and performance of the printed gratings. To mitigate these limitations and ensure high fabrication accuracy, we have systematically optimized the printing parameters, effectively minimizing structural deviations (judged from microscopy images) and enhancing the overall reliability of the fabricated demultiplexers (judged by repeatability of the performance from sample to sample). The paper is organized as follows. First, we discuss the numerical design and optimization of Side-Coupled Waveguide Bragg Grating Filters capable of dropping individual 3 GHz-wide channels with center frequencies in the 140-170 GHz range, while letting other frequencies pass through. Particular attention is paid to the design and fabrication of Waveguide Bragg Gratings [90, 91] which are principal enabling elements of our spectral filters. Then, we discuss the spectral characterization of several such filters using an in-house photonics-based THz communication system [50] . Finally, we show how such filters can be integrated into 3-channel demultiplexers using either in-plane (2D) or out-of-plane (3D) integration strategies and conduct spectral and Bit Error Rate characterization of the resultant devices.

4.4 Design of the WDM THz Filters

Recent advancements in integrated waveguide Bragg grating (WBG) devices have highlighted their potential in microwave and IR for applications such as optical filtering, tunable delays, optical differentiation, and single-sideband modulation. WBG devices offer compactness, flexibility, and high efficiency, making them ideal for applications that require high-performance signal processing. Their ability to operate at THz bandwidths and integrate with other photonic components opens new possibilities for the development of high-speed, low-cost microwave photonic systems [92, 93]. Min-Cheol Oh et al. demonstrated a tunable wavelength filter using Bragg gratings in polymer waveguides, leveraging the thermo-optic effect to efficiently shift the Bragg reflection wavelength. This approach achieved a tuning range of

over 10 nm with low insertion loss [94]. The Side-Coupled Waveguide Bragg Grating Filter used in our work is an integrated photonic device for filtering out a specific wavelength of light. The schematic of such a device is shown in Fig. 4.1. (a). The principle of operation of such a device is as follows. The THz light with a mix of wavelengths (e.g. $\lambda 1$, $\lambda 2$, $\lambda 3$) enters the filter through the In port, propagates through a bend, and encounters a waveguide Bragg grating. Wavelengths that fall outside of the grating stopband stopband (e.g. $\lambda 2$, $\lambda 3$) continue through the grating while being redirected from the top waveguide to the bottom waveguide by the directional coupler, finally exiting the Through port. At the same time, wavelengths falling into the Bragg grating stop band (e.g. $\lambda 1$) are reflected by the grating while being redirected from the top waveguide into the bottom waveguide by the directional coupler, finally exiting at the Drop port.

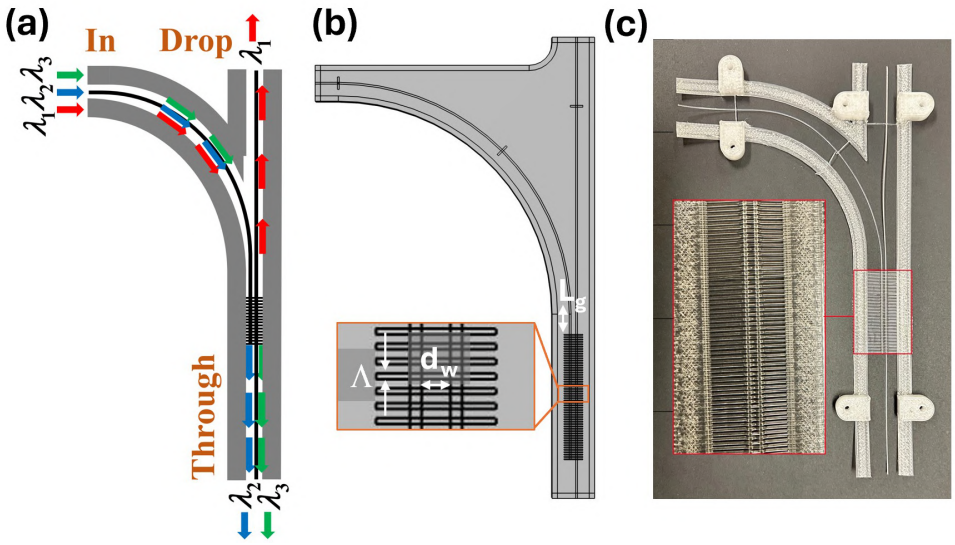

Figure 4.1 (a) A schematic of a WDM demultiplexer (b) A typical computational cell used in numerical simulations. (c) A photo of a WDM demultiplexer. Inset: zoom of a grating section.

The design process for such a filter involves three main steps: designing the Waveguide Bragg Grating, designing the directional coupler, and optimizing the overall structure. The first step is to design the Waveguide Bragg Grating, which is responsible for dropping a specific wavelength. This involves selecting a grating period (Λ) based on the desired drop frequency. The period is chosen to ensure that the Bragg grating stop band is centered around one of the channel carrier frequencies (e.g. 140 GHz). The second step involves designing a directional coupler, which includes a circular arc, and two waveguides running directly under the Bragg Grating. First, a separation distance dw between two parallel waveguides is set to result in a relatively short device that can be printed using a 30 cm x 30 cm build plate of a 3D

printer. Smaller values of dw result in stronger coupling between two waveguides, and, thus, smaller device size. Next, the number of grating periods Ng is estimated to achieve near-zero transmission for wavelengths within the grating stop band. The exact number of periods in the grating is chosen, so that a second channel outside of the grating stop band (e.g. 145 GHz) is diverted from the launch waveguide into the Through port of a coupler. Finally, the standoff distance between the bend termination and the grating Lg is chosen so that the intensity in the Drop port is maximized at the center frequency of a dropped channel. To perform optimizations, we used finite element COMSOL Multiphysics software with a typical computation cell shown in Fig. 4.1 (b).

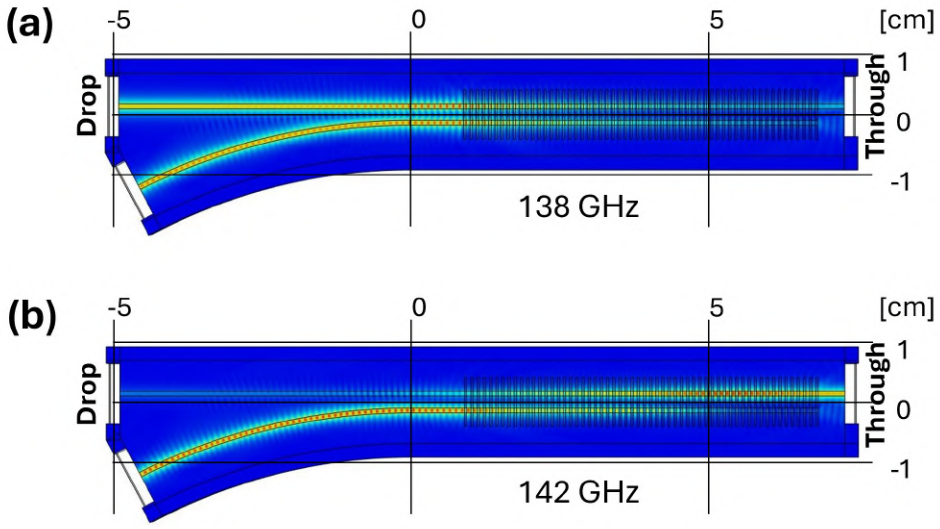

Figure 4.2 Electric field amplitude distribution in the Demux1 operating at (a) Drop (138 GHz) and (b) Through (142 GHz) frequencies.

Three devices were numerically optimized to have Drop channels centered around 138 GHz, 142 GHz, and 146 GHz, with the Through frequencies 4GHz above the Drop channel center frequencies. In Fig 4.2 electric field amplitude distributions are shown for Demux1 operating at the Drop (138 GHz) (panel a)) and Through (142 GHz) frequencies (panel b)) [9, 10]. Drop and Through transmission coefficients (by power) are shown in Fig 4.4 (a) and (b) (computed using numerical cells shown in Fig. 2). Finally, the geometric parameters of three multiplexers including the grating period, the number of grating periods, the distance between two parallel waveguides, and the standoff distance between the bend termination and the grating are summarized in Table 4.1.

Table 4.1 Geometrical parameters of the demultiplexers

Parameter	**Demux 1**	**Demux 2**	**Demux 3**
Center frequency (GHz)	138	142	146
Grating period Λ (μm)	1020	984	949
Number of periods	57	63	76
Waveguide distance d_W (mm)	1.95	1.95	1.95
Standoff distance L_g (mm)	9	15	21

4.5 Experimental realization of the WDM THz Filters

The experimental realization of thus designed filters is challenging. The difficulty arises from the need for precise alignment of the waveguide Bragg grating relative to the waveguide coupler and providing mechanical support for the suspended-in-air components of the structure. To this end, the filter components are printed within a rigid hollow frame that features several slender support elements. The first printed layer contains slender support attached to the frame. The second layer contains all the waveguides printed on top of the supports using a 0.8mm diameter nozzle. Finally, the third layer contains Bragg grating printed on top of the waveguide layer using a 0.4 mm diameter nozzle. The grating extends to the support frame for mechanical stability. To splice several filters together a 1mm-diameter glass capillary of 100um wall thickness is used to align and put in contact the Through and In waveguides of the two filters. The capillary is then heated to fuse the plastic waveguides and then removed by shattering. Finally, the device is assembled on the optical bench with the frame kept under light tension using alignment screws. A photo of a typical demultiplexer is shown in Fig. 4.1 (c).

4.6 Optical Characterization of the WDM THz Filters

Optical characterization of the 3D-printed demultiplexers was conducted using an in-house photonics-based THz communication system detailed earlier [48]. The schematic of the optical characterization setup is presented in Fig. 3(a), while Fig. 4.3(c) shows a photo of the measurement setup with a mounted device. Briefly, in the transmitter arm, two DFB lasers, independently tunable and operating within the infrared C-band with somewhat mismatched center frequencies, are combined using a 3 dB coupler and sent to a fiber-coupled photomixer to generate THz waves of fixed frequency anywhere in the 0.1-1 THz range with bandwidth of 10MHz. In the THz CW spectroscopy mode: the THz radiation of a set frequency from the photomixer (Model: IOD-PMD-14001 from NTT Electronics Inc) is guided through a WR-

6 rectangular waveguide flange [see Fig. 4.3(a)], which is butt-coupled to the device under study. On the receiving end, a 10.8 mm diameter horn antenna collects the THz waves, which are then detected using a zero-bias Schottky detector (Model: WR8.0 ZBD-F from Virginia Diodes Inc). A high-gain, low-noise amplifier (Model: SLNA-030-32-30-SMA from Fairview Microwave Inc) is then used to amplify the received signal for further processing. In the THz communication mode [see Fig. 4.3 (b)]: a baseband signal source, generated by a pulse pattern generator integrated into the test equipment, produces pseudorandom bit sequences with varying bit rates. This signal undergoes amplification and modulation utilizing RF and Mach-Zhender modulation techniques. The modulated laser beams are further amplified and injected into a photomixer to generate a modulated THz carrier wave. In the receiver section, the THz carrier wave is detected and demodulated using a zero-bias Schottky diode, then amplified through a low-noise amplifier. Eye pattern and bit error rate (BER) are then recorded. In more details, at the emitter side, the combined infrared optical signal from the coupler is modulated using an external electro-optic modulator (Models: LN81S-FC and MX10A from Thorlabs Inc). The modulated optical signal, with a fixed output power, is then amplified using an Erbium-Doped Fiber Amplifier (EDFA). At the receiver side, a Bias-Tee filters the DC field from the demodulated baseband signal, and a low-noise amplifier (LNA) further amplifies the received signal. Finally, the demodulated baseband signals are analyzed using a high-speed oscilloscope and a BER tester (Model: MP2100B from Anritsu Corporation). The BER measurements were conducted by varying the bit rate from 1 Gbps to 6 Gbps or adjusting the carrier frequency at a fixed bit rate. At each bit rate or carrier frequency, the decision threshold was optimized to balance insertion errors (digital zero misidentified as one) and omission errors (digital one misidentified as zero), thereby minimizing the BER.

In the experiments, the THz carrier wave in the 120 – 165 GHz spectral range was generated using an optical photomixer (IOD-PMD-14001, NTT Electronics) with a photocurrent of 7mA generating THz powers between 125 µW (-9 dBm) and 250 µW(-6 dBm), and then coupled into a demultiplexer via a 1-inch-long WR6.5 rectangular waveguide terminated with a horn (WR8.0 ZBD-F, Virginia Diodes). A similar configuration was utilized at the output port of a demultiplexer where a horn was connected via a 1-inch-long WR6.5 rectangular waveguide to the Schottky diode. Operation of the Drop and Through ports of the filters were then characterized using two complimentary measurement modes, namely, THz CW spectroscopy and BER characterization for data transmission [9, 10]. First, CW THz spectroscopy was conducted on three demultiplexers without data modulation. To extract the relative Drop and Trough coefficients (shown in Figs. 4.4(c,d)) for direct comparison with theoretical predictions (computed using numerical cells shown in Fig. 4.2) we normalize the raw transmission data by the transmission of a stand-alone bent waveguide (Rb=10 cm,

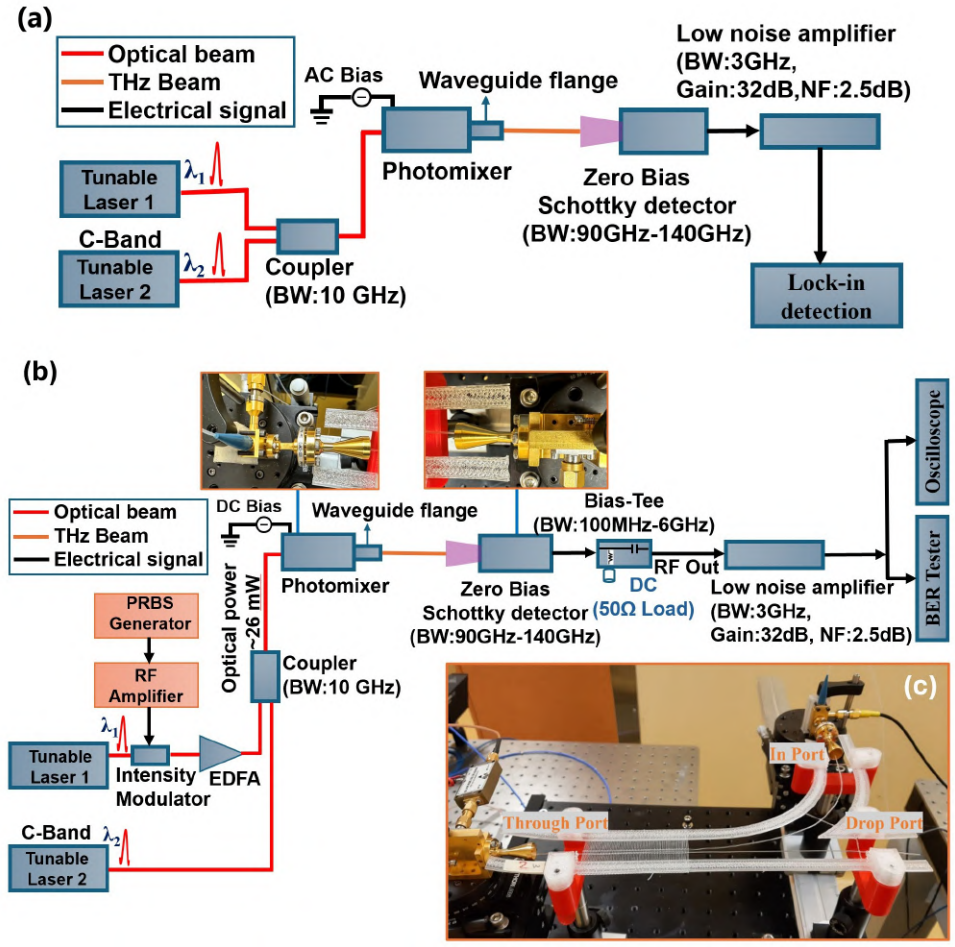

Figure 4.3 a) Schematic of the Continuous Wave THz spectroscopy system. (b) Schematic of the photonics-based THz communication system. (c) Photo of the measurement setup with a mounted device.

90o-bend) identical to those used in the filters (see insert in Fig. 4.4(c)). We note that overall, numerically computed spectra (shown in Figs. 4(a,b)) have very similar shapes to the measured ones. Additionally, as per the design goal, the higher-frequency edge of the Trough spectra shows higher transmission than the lower-frequency edge. At the same time, the experimental spectra are shifted to higher frequencies by several GHz. Moreover, we observe strong sidelobe suppression outside of the stopband in experimental spectra which results in the 6 GHz experimental bandwidths at the Drop port, which is somewhat larger than numerically predicted bandwidths of 4 GHz. Finally, the maximal amplitudes of the measured Drop spectra are somewhat lower (0.5-0.6) compared to the theoretical ones (0.8), due to scattering losses on supporting structures (10% scattering loss per structure predicted numerically using numerical cell shown in Fig. 4.1(b)), as well as due to nonuniformities of 3D-printed waveguides including wall roughness and micro-bending. The overall insertion

loss is estimated to be 1.7 dB for the Drop port, and 1 dB for the Through port, which implies that with even a modest power budget of 11 dB, one can build a 10-channel THz WDM system using such filters placed in sequence.

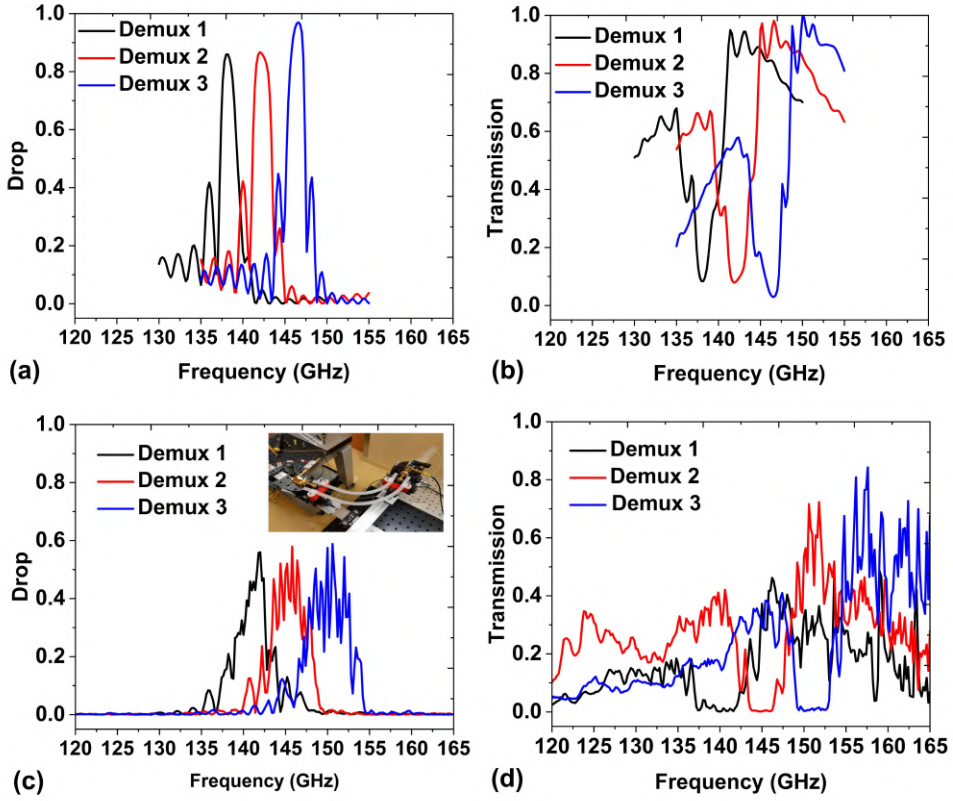

Figure 4.4 (a) Drop and (b) Through spectra as predicted by numerical simulations. Relative (c) Drop and (d) Through coefficients when using transmission through a stand-alone bend as a reference. Insert: picture of a stand-alone waveguide bend [9, 10].

Next, we characterize information transmission through the 3 thus-developed multiplexors. Using Fig. 4.4, we chose the channel center frequencies as follows: demultiplexer 1 (Drop 140 GHz, Through 145 GHz), demultiplexer 2 (Drop 145 GHz, Through 150 GHz), and demultiplexer 3 (Drop 150 GHz, Through 155 GHz). Therefore, all the following BER measurements will be conducted at those frequencies. Specifically, the eye patterns for the THz data streams of various bit rates ranging from 1 to 6 Gbps using amplitude-shift-keying modulation were recorded, and corresponding Bit Error Rate (BER) measurements were conducted. During BER measurements, the decision threshold was adjusted to balance the insertion error (incorrectly identifying a digital 0 as a digital 1) and omission error (incorrectly identifying a digital 1 as a digital 0). The duration of recording was determined as 1/(target BER $\times$ bit rate), with the target BER set to 10-12 (error-free transmission threshold). First,

the performance of Demux1 was characterized in the Drop mode at the carrier frequency corresponding to the grating stopband center frequency of 140 GHz. Next, the performance of Demux1 was characterized in the Through mode using the carrier outside of the grating stopband at 145 GHz as shown in Fig. 4.5(a). Similarly, performances of Demux2 and Demux3 were characterized in Drop mode at the corresponding stopband center frequencies of 145 GHz and 150 GHz, as well as in Through mode outside of the corresponding stopbands at 150 GHz and 155 GHz as shown in Figs. 4.5(b,c). Experimental data confirms that all demultiplexers can operate with 6Gbps data streams with BER<10^{-4} below the forward error correction limit of 10^{-3}.

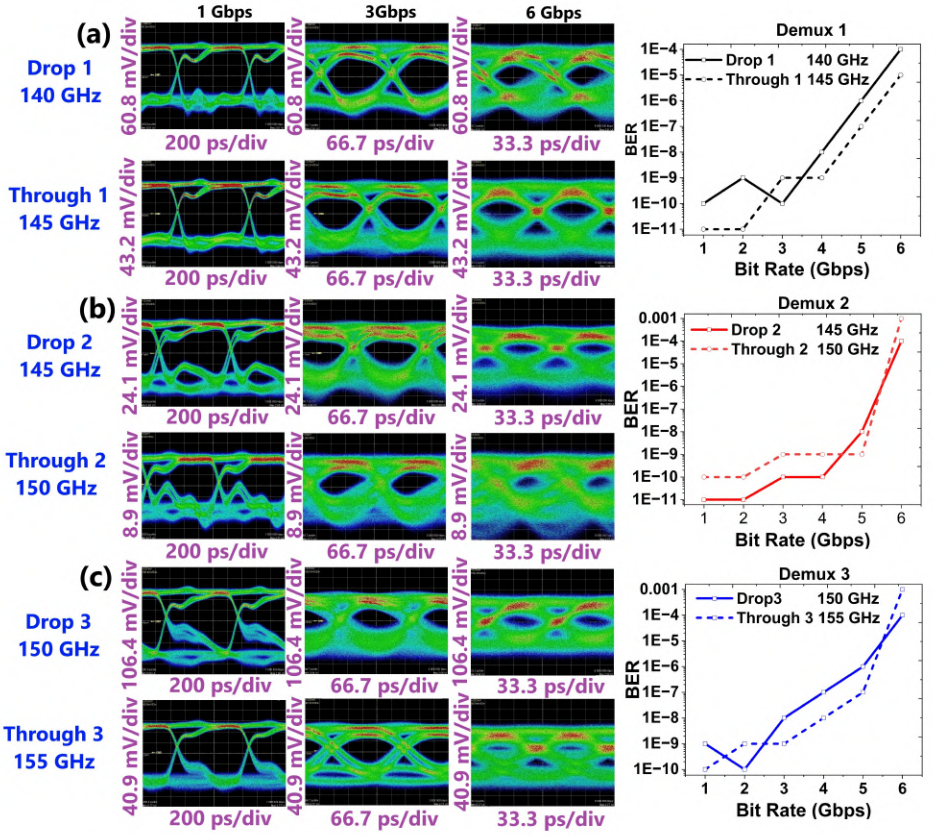

Figure 4.5 Measured Bit Error Rate (BER) versus Bit Rate in the 1-6 GBps range and the corresponding eye diagrams for 3 demultiplexers (a) Demux1 (b) Demux2, and (c) Demux3 at the Drop and Through ports [9, 10].

4.6.1 WDM Devices – Two Demultiplexers Connected in Sequence

In the following, we demonstrate 3-channel demultiplexers using two filters from the previous section connected in sequence (schematically shown in Fig. 4.6(a)). The first device was made

by splicing the Through 1 and In 2 ports of Demux 1 and Demux 2 (Demux 1+2), while the second one was made by splicing the Through 2 and In 3 ports of Demux 2 with Demux 3 (Demux 2+3) as shown in Fig. 6(b). Then, spectroscopic and BER measurements were performed at various Drop and Through ports.

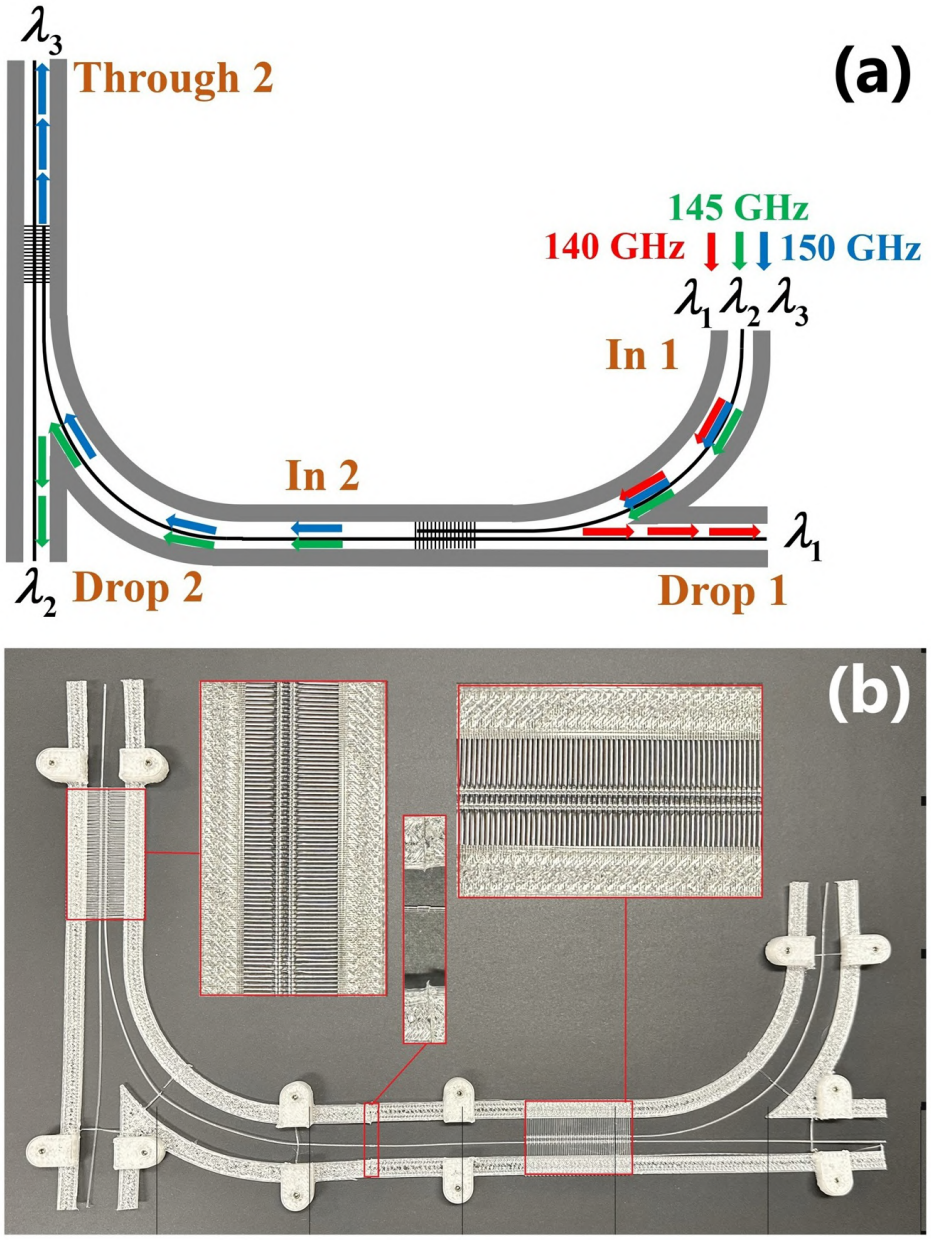

Figure 4.6 a) A schematic of the in-sequence demultiplexer (Demux 1+2). (b) A photo of the assembled device.

Fig. 4.7 (a) shows the Drop 1 spectrum, while Fig. 4.7 (b) shows Drop 2/Through 2 spectra in the range of 120–165 GHz for Demux 1+2. Similarly, Fig. 4.7 (c) shows the Drop 2

spectrum, while Fig. 8 (d) shows Drop 3 and Through 3 spectra for Demux 1+3.

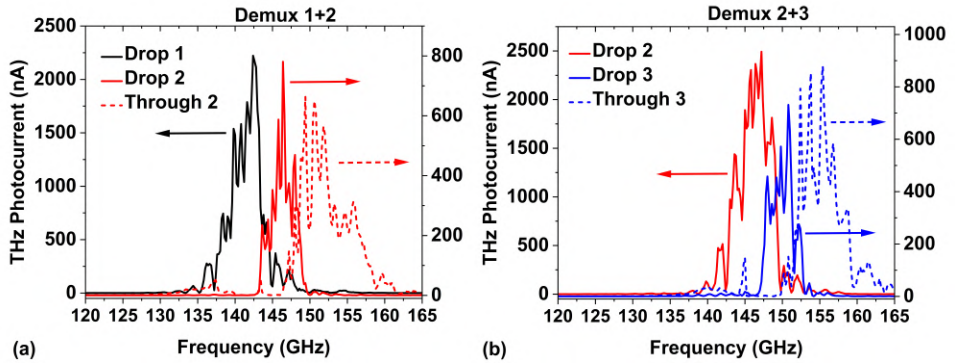

Figure 4.7 Experimental spectra of (a) Drop 1, (b) Drop 2, and Through 2 of the Demux 1+2. Experimental spectra of (c) Drop 2, (d) Drop 3, and Through 3 of the Demux 2+3.

The communication performance of in-sequence demultiplexers was evaluated by measuring the bit error rate (BER) while adjusting the bit rate from 1 to 6 Gbps. Specifically, for Demux 1+2, BER was measured at 140 GHz for the Drop 1 port, 145 GHz for the Drop 2, and 150 GHz for the Through 2 ports. The measured bit error rate (BER) versus bit rate, along with the corresponding eye diagrams for Demux 1+2 are shown in Figure 4.8 (a-d). Similarly, for Demux 2+3 BER was measured at 145 GHz for the Drop 1 port, 150 GHz for the Drop 3 port, and 155 GHz for the Through 3 port. The measured BER versus bit rate, along with the corresponding eye diagrams, are presented in Figure 4.8 (d-h).

4.6.2 WDM Devices – Two Demultiplexers Connected in Parallel

Finally, we demonstrate 3-channel demultiplexers using two filters connected in parallel (schematically shown in Fig. 4.9(a)). The first device was made by splicing the In and Through ports of Demux 1 and Demux 2 (Demux 1||2), while the second one was made by splicing the In and Through ports of Demux 2 with Demux 3 (Demux 2||3) as shown in Fig. 4.9(b). Then, spectroscopic and BER measurements were performed at various Drop and Through ports.

Experimental spectra at the Drop 1, Drop 2, and Through 1+2 ports of the in-parallel Demux 1||2 are shown in Fig. 4.10 (a) in the spectral range of 120–165 GHz. Similarly, experimental spectra at the Drop 2, Drop 3, and Through 2+3 ports of the in-parallel Demux 2||3 are shown in Fig. 4.10 (b).

The communication performance of the in-parallel Demux 1||2 was evaluated by measuring the bit error rate (BER) for bit rates between 1 and 6 Gbps. Specifically, BER was measured

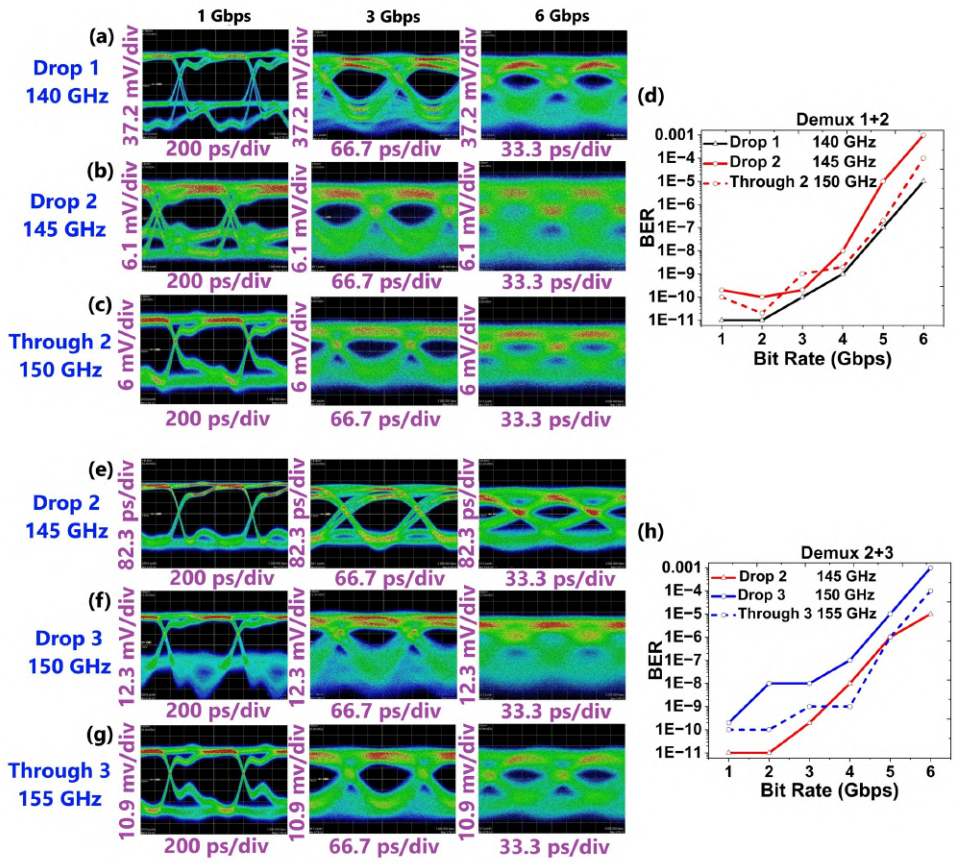

Figure 4.8 Measured Bit Error Rate versus Bit Rate and the corresponding eye diagrams for in-sequence Demux 1+2 at different bitrates (a) eye pattern at the Drop 1 port (b) eye pattern at the Drop 2 port (c) eye pattern at the Through 2 port (d) BER at the Drop 1, Drop 2, and Through 2 ports. Similar data is shown in panels (e)-(h) for Demux 2+3 and ports Drop 2, Drop 3, and Through 3 ports.

at 140 GHz for Drop 1, 145 GHz for Drop 2, and 140 GHz, 145 GHz, and 150 GHz for the composite Through 1+2 ports. The measured bit error rate (BER) versus bit rate, along with the corresponding eye diagrams for the Demux 2|3 are shown in Figs. 4.11 (a-d). Similarly, for Demux 2|3 BER was measured at 145 GHz for Drop 1, 150 GHz for Drop 3, and 145 GHz, 150 GHz, and 155 GHz for Through 2+3 ports. The measured BER versus bit rate, along with the corresponding eye diagrams, are presented in Figs. 4.11 (e-h).

4.7 Conclusion

In this work, three THz demultiplexer filters, as well as their combinations in sequence and in parallel were fabricated and characterized for operation with four sub-mm wave channels (140

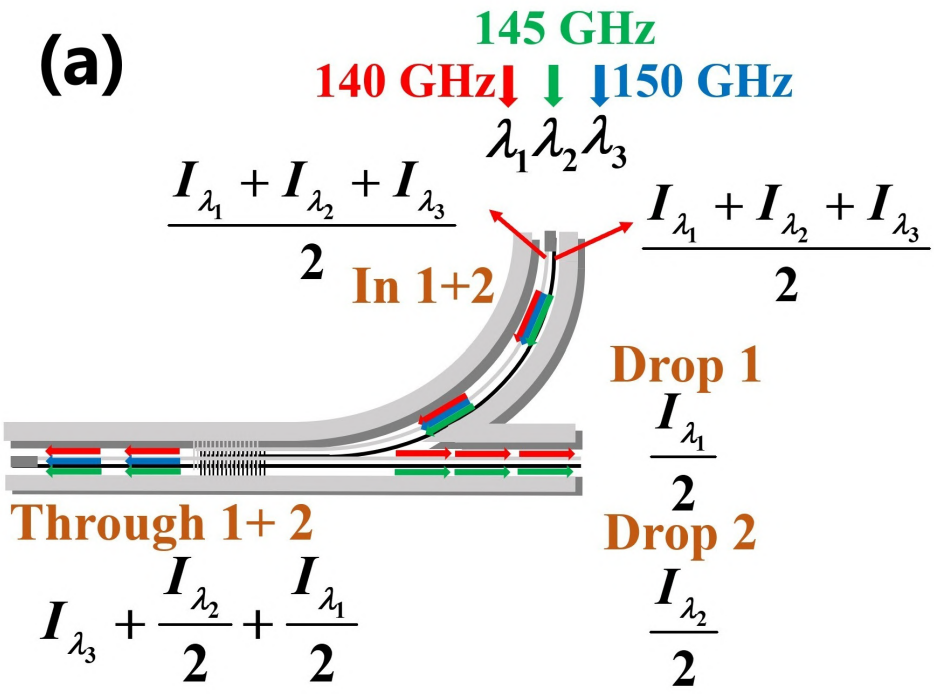

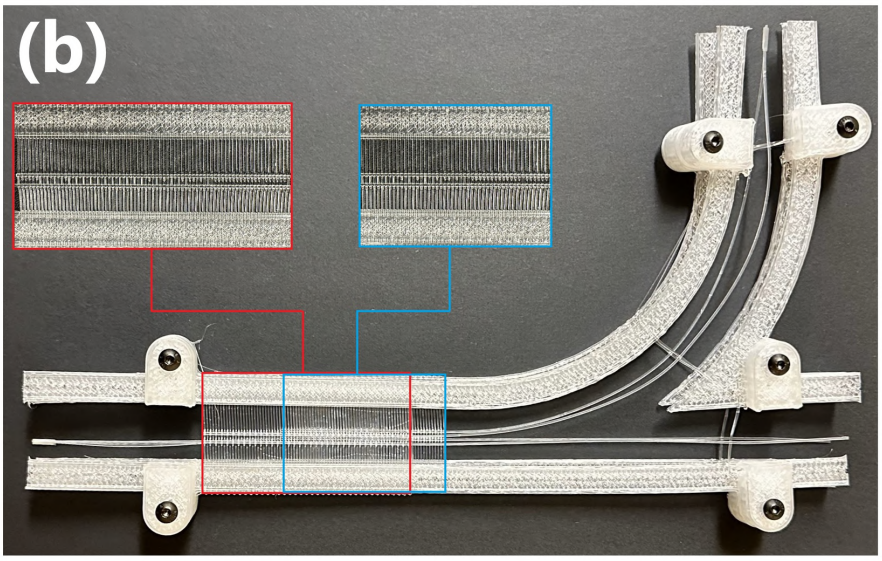

Figure 4.9 A schematic of the in-parallel demultiplexer (Demux 1||2). (b) A photo of the assembled device.

GHz, 145 GHz, 150 GHz, and 155 GHz) within the WDM framework of Terahertz Communication. Successful channel demultiplexing of 3 channels per device was demonstrated with up to 6Gbps data rates. Experimental results further demonstrate strong sidelobe suppression and a broader Drop port bandwidth (6 GHz compared to the predicted 4 GHz). However, the measured Drop amplitudes (0.5–0.6) are lower than the theoretical predictions (0.8),

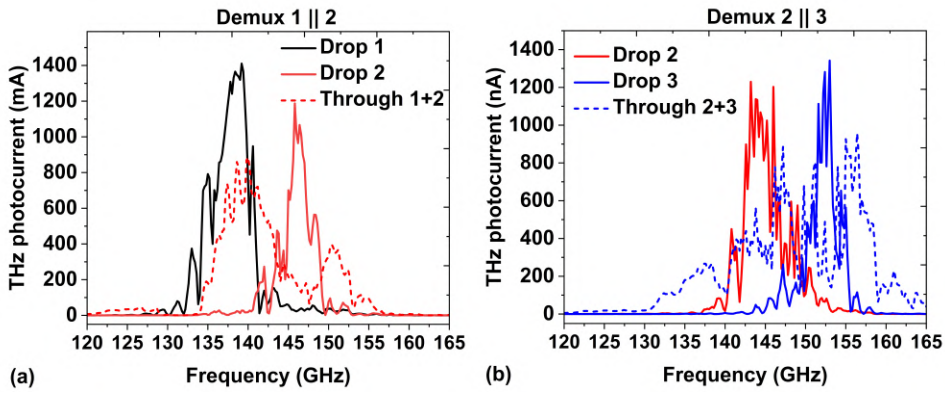

Figure 4.10 Experimental Drop 1, Drop 2, and Through 1+2 spectra of the Demux 1||2. (b) Experimental Drop 2, Drop 3, and Through 2+3 spectra of the Demux 2||3.

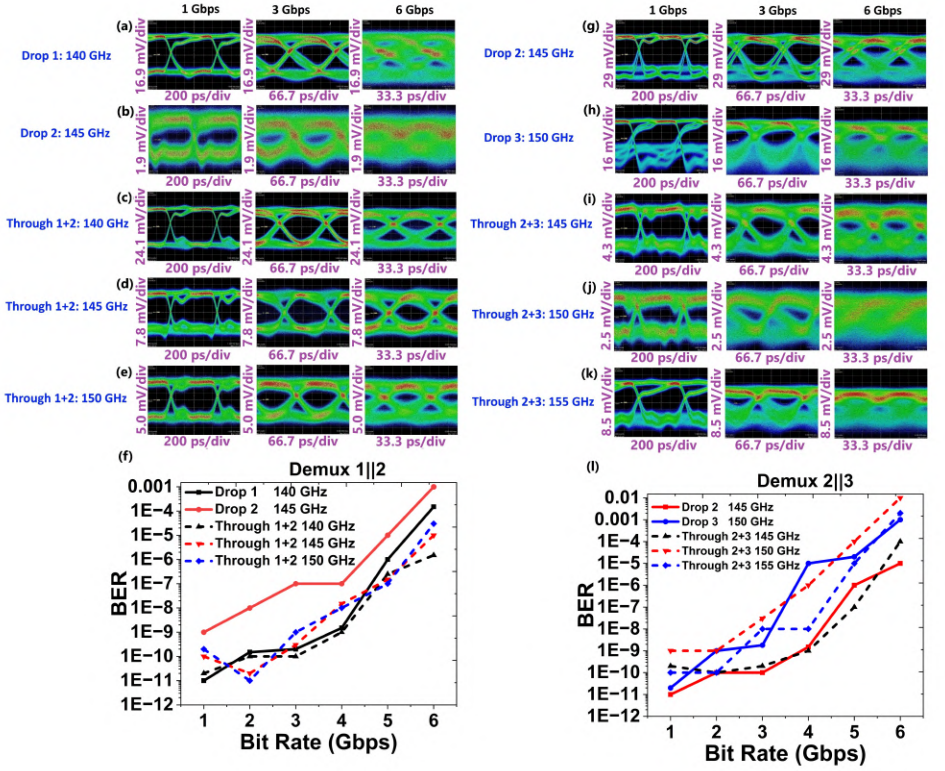

Figure 4.11 Measured Bit Error Rate versus Bit Rate and the corresponding eye diagrams for in-parallel Demux 1||2 at different bitrates. Eye patterns at the (a) Drop 1 port, (b) Drop 2 port, (c,d,e) Through 1+2 port. (e) BER at the Drop 1, Drop 2, and Through 1+2 ports. Similar data is shown in panels (g)-(l) for Demux 2||3 and ports Drop 2, Drop 3, and Through 2+3.

primarily due to approximately 10% scattering losses per supporting structure. Our study indicates that additive manufacturing of THz circuits with a high-refractive-index-contrast Polypropylene-in-air material combination presents a viable approach for high-quality low-loss fabrication of integrated THz devices. Additionally, additive manufacturing carries a strong potential for three-dimensional integration of THz circuits, as well as a fast turn-around between design and prototyping.

4.8 Acknowledgement

The authors wish to acknowledge the funding from the NSERC Discovery Grant of Prof. Maksim Skorobogatiy to carry out this project.

CHAPTER 5 CONFERENCE PRESENTATIONS

The research conducted in this thesis led to the following peer-reviewed conference presentations, which received recognition for their quality and contribution.

1- **Yahyapour, Babak**, Frederic Marcotte, Roya Gachiloo, and Maksim Skorobogatiy. "Terahertz Demultiplexers Suspended in Air using 3D Printing Technique." In 2025 IEEE 15th Annual Computing and Communication Workshop and Conference (CCWC), pp. 01021-01023. IEEE, 2025.

This paper was honoured with the **Best Paper Award** at the 2025 IEEE 15th Annual Computing and Communication Workshop and Conference (CCWC).

2- **Yahyapour, Babak**, Frederic Marcotte, Roya Gachiloo, and Maksim Skorobogatiy. "3D Printed THz Demultiplexer Circuits Using Suspended-in-Air Grating Couplers." In 2025 IEEE International Conference on Consumer Electronics (ICCE), pp. 1-3. IEEE, 2025.

This paper received the **Best Presentation Award** at the 2025 IEEE International Conference on Consumer Electronics (ICCE).

3- **Yahyapour, Babak**, Frederic Marcotte, Roya Gachiloo, and Maksim Skorobogatiy."3D Printed Three Channel WDM Demultiplexers Using Low-Loss Splicing Technique for THz Communication Systems." Presented at the Annual Conference - COPL - Summer School, 2025.

This presentation received the **Best Poster Award** at the Annual Conference - COPL - Summer School, 2025.

These conference presentations highlight my research contributions to advancing terahertz communication systems through the development of innovative 3D-printed demultiplexer circuits.

CHAPTER 6 GENERAL DISCUSSION

This chapter discusses the practical challenges encountered during the fabrication and integration of the 3D-printed terahertz demultiplexers. While the previous chapters presented the successful design and performance of the devices, the focus here is on the challenges within the manufacturing process.

6.1 Optimization of print quality using a standard Fused Deposition Modeling (FDM) printer

Next, the multiparameter optimization of the FDM printing process is presented and discussed. The Fused Deposition Modeling (FDM) technique inherently introduces surface roughness on the scale of the deposited layer thickness. Additionally, when printing fiber bulk regions at 100% volume filling, accidental air trapping can occur. Both surface roughness and trapped air contribute to additional scattering losses. However, at low THz frequencies—most relevant for communication applications—the typical wavelength is approximately 1mm, while the layer thickness and transverse resolution of an FDM printer are on the order of 0.1mm. Thus, the surface and bulk roughness are deeply subwavelength, and scattering from such defects is expected to follow Rayleigh scattering laws. A "Raise3D Pro3" FDM printer, offering high positional precision (1 µm in the XY plane and 10µm along the Z-axis), was employed. Natural transparent polypropylene (PP) filament with a diameter of 1.75mm was selected due to its high transparency and low absorption in the THz regime . A standard "Rectilinear" infill pattern was used during optimization, as it generally produces mechanically isotropic prints in the build plane. The optimal extrusion temperature for polypropylene is reported to be in the 190–250°C range [95]; in this study, 240°C was selected in accordance with the filament manufacturer's recommendations. Polypropylene's high coefficient of thermal shrinkage makes it highly susceptible to warping, leading to the corners of the print detaching from the build plate. This is catastrophic for a device that requires precise alignment, like our demultiplexer. Maintaining a consistent, elevated chamber temperature (100°C for the build plate, 50°C for the enclosure) was essential to reduce the thermal gradient between the newly extruded layer and the solidified layers below, thereby minimizing internal stresses.

6.1.1 Optimization of Nozzle and Printing Parameters

The use of a 0.8 mm-diameter nozzle for the large waveguide structures enabled faster printing and robust mechanical layers. Switching to a 0.4 mm nozzle for the Bragg grating was imperative to achieve the fine feature definition required for the 1 mm period gratings. We found that reducing the print speed for the grating sections to 20 mm/s and carefully calibrating the extrusion multiplier (flow rate) was necessary to achieve the target filament width. Over-extrusion would blur the grating features, while under-extrusion would create weak, discontinuous segments. A layer height of 0.2 mm provided a good balance between print resolution and strength. Furthermore, we minimized the part-cooling fan speed for polypropylene to encourage layer-to-layer adhesion and reduce the risk of delamination, a standard failure mode in tall, slender support structures. In conclusion, the successful demonstration of the 3D-printed THz demultiplexers also required overcoming significant fabrication hurdles. The challenges of splicing and integration highlight the need for future work on monolithically printed multi-channel devices to avoid assembly losses. Simultaneously, the extensive print parameter optimization outlined a reproducible procedure for fabricating high-quality, suspended THz circuits, establishing a valuable framework for the continued development of additive manufacturing in terahertz photonics.

6.2 Technical challenges

During the development of 3D-printed terahertz (THz) demultiplexers using suspended-in-air grating couplers, several technical challenges were encountered, each requiring attention to ensure the final devices met the desired performance specifications. These challenges spanned the design, fabrication, and experimental validation stages of the project, demanding a careful balance between innovative design solutions, precise fabrication techniques, and rigorous testing protocols. One of the most significant challenges during fabrication was achieving the required accuracy and precision in printing waveguides and grating structures. While 3D printing offers remarkable flexibility in geometric design, it also introduces inherent limitations in dimensional accuracy. Factors such as warping, adhesion issues, and inconsistent filament extrusion created challenges in producing components that met the necessary tolerances for high-performance THz devices. Warping is a common issue in 3D printing, especially with thermoplastic materials like polypropylene. As the printed layers cooled, they tended to contract, causing warping that distorted the geometry of the waveguides and grating filters. This issue had the potential to significantly affect the devices' efficiency and functionality, leading to increased scattering losses and reduced transmission quality. To mitigate these effects, the printing parameters had to be optimized, including the extrusion speed, nozzle

diameter, and layer thickness. Additionally, thermal management during printing was critical, as temperature fluctuations in the printing environment could exacerbate these issues. Another challenge stemmed from the unique design of the grating couplers, which were suspended in air to achieve high refractive-index contrast. This innovative approach required careful mechanical support for the suspended components, as they needed to remain stable during printing and in the final device. The mechanical support structures had to be both robust enough to prevent distortion during printing and small enough to avoid interfering with the optical paths once the components were integrated into a functional device. To address this, the design incorporated slender support elements integrated into a rigid frame, providing the necessary stability without excessive bulk. Aligning the grating couplers with the waveguides during printing was a delicate process, as even slight misalignments could degrade filter performance. This challenge was particularly pronounced when integrating the components into a single device, where precise alignment was crucial to achieve the desired optical performance. The mechanical supports also had to be designed to withstand any stresses during fabrication, ensuring that the suspended grating structures did not shift or distort. The design of the Waveguide Bragg Gratings (WBG) and directional couplers presented additional hurdles. These components are fundamental to the demultiplexer's ability to filter specific wavelengths and separate the THz channels. The challenge lay in optimizing the grating period and the number of grating periods to ensure the filter effectively dropped a particular wavelength while allowing other wavelengths to pass. Numerical simulations played a crucial role in this process, enabling precise tuning of parameters such as the grating period and inter-waveguide distance. However, achieving the optimal configuration required iterative design adjustments, particularly in balancing the trade-off between device size and coupling efficiency. Smaller grating periods enabled more compact devices but also increased waveguide coupling, which in turn affected device performance. Optimizing these parameters for the 120-165 GHz frequency range, with minimal losses and high efficiency, was a technically demanding task.

Once the components were designed and printed, the integration into fully functional devices presented its own set of challenges. The printed filters, couplers, and waveguides had to be aligned and spliced together to create the demultiplexer. This integration process required splicing the Through and In ports of adjacent filters, which was a delicate operation. The challenge was not only to connect the components physically, but also to ensure that the splice did not introduce significant losses or misalignments. The low-loss splicing technique employed, which used a 1 mm-diameter glass capillary to align and fuse the waveguides, was effective, but it required careful temperature control during the fusion process to avoid damage to the printed components. The final demultiplexer assemblies were then mounted on an

optical bench, where the mechanical stability of the entire structure was crucial for maintaining alignment and ensuring proper device operation. Once assembled, the demultiplexers were subjected to experimental validation to assess their performance. The bit error rate (BER) measurements, conducted over a range of data rates up to 6 Gbps, revealed several discrepancies between the predicted and actual device performance. The measured drop amplitudes were lower than the theoretical predictions, which was attributed to several factors, including scattering losses from the support structures and micro-bending in the printed waveguides. The scattering losses occurred at the points where the components were supported, as the structures themselves contributed to energy dissipation. Additionally, variations in waveguide quality, such as wall roughness and slight misalignments during printing, introduced imperfections that degraded signal quality. These challenges were particularly evident in the sidelobe suppression and bandwidth of the drop ports. While theoretical predictions suggested a narrower bandwidth, experimental results showed a broader bandwidth, suggesting that some simulation parameters did not fully capture the complexities of the printed devices. Furthermore, the frequency shift observed in the experimental spectra, where the measured frequencies were slightly higher than the simulated ones, indicated a mismatch in the refractive index of the printed material, which could have been influenced by slight variations in the printing process or by the thermal properties of the polypropylene. These discrepancies between simulation and experiment underscore the need to continuously refine printing and design processes to ensure devices perform as expected in real-world applications. Finally, scalability and cost-effectiveness were critical considerations for the successful application of 3D printing in the development of THz devices. While the use of polypropylene and the FDM printing process enabled relatively low-cost fabrication and rapid prototyping, there were still limitations on the maximum device size that could be printed and the resolution of the printed components. The process also required ongoing optimization to ensure that larger-scale devices could be fabricated with the same level of accuracy and reliability. In summary, the challenges encountered in this project were multifaceted, encompassing fabrication accuracy, component integration, and performance validation. Despite these obstacles, significant progress was made in demonstrating the feasibility of 3D printing for THz demultiplexer development, and the solutions developed to address these challenges have the potential to pave the way for more advanced, scalable, and cost-effective THz communication devices in the future.

6.3 Challenges in Sequentially and Parallel-Connected 3D-Printed THz Demultiplexers

In particular, this section discusses the complexities of connecting multiple demultiplexers using the custom splicing technique, as well as the systematic optimizations required to achieve high-quality prints with a Fused Deposition Modeling (FDM) printer. A key objective of this work was to move beyond single filters and demonstrate multi-channel systems by connecting individual demultiplexers in sequence and in parallel. The splicing technique, while enabling this integration, introduced several significant challenges.

The splicing process, which involved aligning waveguides using a 1mm-diameter glass capillary and thermally fusing them, represented a critical bottleneck. The primary challenge was achieving and maintaining sub-millimeter axial and angular alignment between the "Through" port of one demultiplexer and the "In" port of the next. Even minor misalignments at these junctions caused several issues: imperfect alignment led to a mismatch in the fundamental mode fields of the connecting waveguides, resulting in significant insertion loss at the splice point. Part of the THz radiation was scattered into higher-order or radiation modes rather than efficiently coupled into the subsequent device.

In sequentially connected demultiplexers (e.g., Demux1+2), the cumulative effect of splice losses and potential misalignments could distort the spectral response. For example, the transmission spectrum for Drop2 in Demux1+2 depended not only on Demux2's intrinsic performance but also on the signal quality it received from Demux1 after the first splice. Consequently, the performance of later stages in a cascade was increasingly sensitive to imperfections in the earlier stages.

Although fused, the spliced joint remained a mechanical weak point. The assembled device was sensitive to external vibrations and handling, which could compromise the precise alignment achieved during careful assembly on the optical bench.

Integrating demultiplexers in parallel (e.g., Demux 1$\|$2) introduced additional challenges related to signal integrity. In this configuration, the composite "Through" port (Through1+2) must transmit a broad spectrum containing all channels not dropped by the individual filters. Due to the finite extinction ratio of each Drop filter, a small fraction of a “dropped” channel could leak into the common Through port. To mitigate this issue, the two parallel demultiplexers must be precisely aligned on the holder.

6.4 Experimental splicing procedure for straight and bent waveguides

The reference signal was identified by aligning the emitter and detector face to face. Measurements were then performed with separations of 5 mm and 10 mm between them. The measured signals are shown in Figure 6.1. To perform the splicing technique, we first mea-

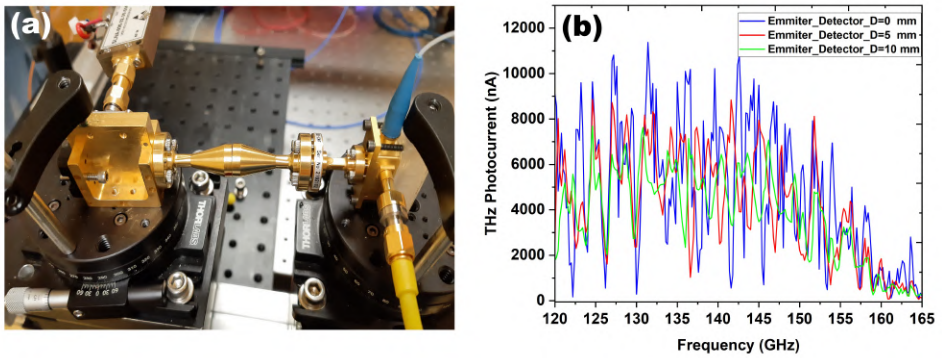

Figure 6.1 Measured reference signals for emitter–detector separations of 5 mm and 10 mm.

sured the straight and bent waveguides. The waveguides were then cut and reconnected using a glass capillary and an electric lighter. Our observations indicate that no significant additional loss was introduced by the splicing process.

Figure 6.2 (a) shows a photograph of the straight waveguide with the experimental setup , and figure 6.2 (b) presents the measured spectra of the straight waveguide before and after cutting.

Figure 6.3 (a-b) shows a photograph of the bent waveguide with the experimental setup, and compares the measured spectra of the bent waveguide before and after cutting.

Figure 6.4 shows the measured transmission spectra at the Through port for the three demultiplexers, together with two reference measurements. First, the response of a 10-cm, 90° bent polypropylene waveguide without any grating is recorded (“Bent”), which serves as a reference for the propagation and coupling losses of the devices. Next, a structure comprising the bent waveguide plus an unloaded grating section (“Bent + grating”) is measured to isolate the impact of the grating itself, in the absence of the side-coupled drop waveguide. The spectra of Demux 1–3 then demonstrate how introducing the directional coupler and Bragg grating produces deep, frequency-selective notches in the Through port around 140, 145, and 150 GHz, corresponding to the designed stopbands of the three filters.

Figure 6.5 presents the corresponding spectra measured at the Drop ports of Demux 1–3. For each device, a broad passband of approximately 6 GHz appears at the frequency where

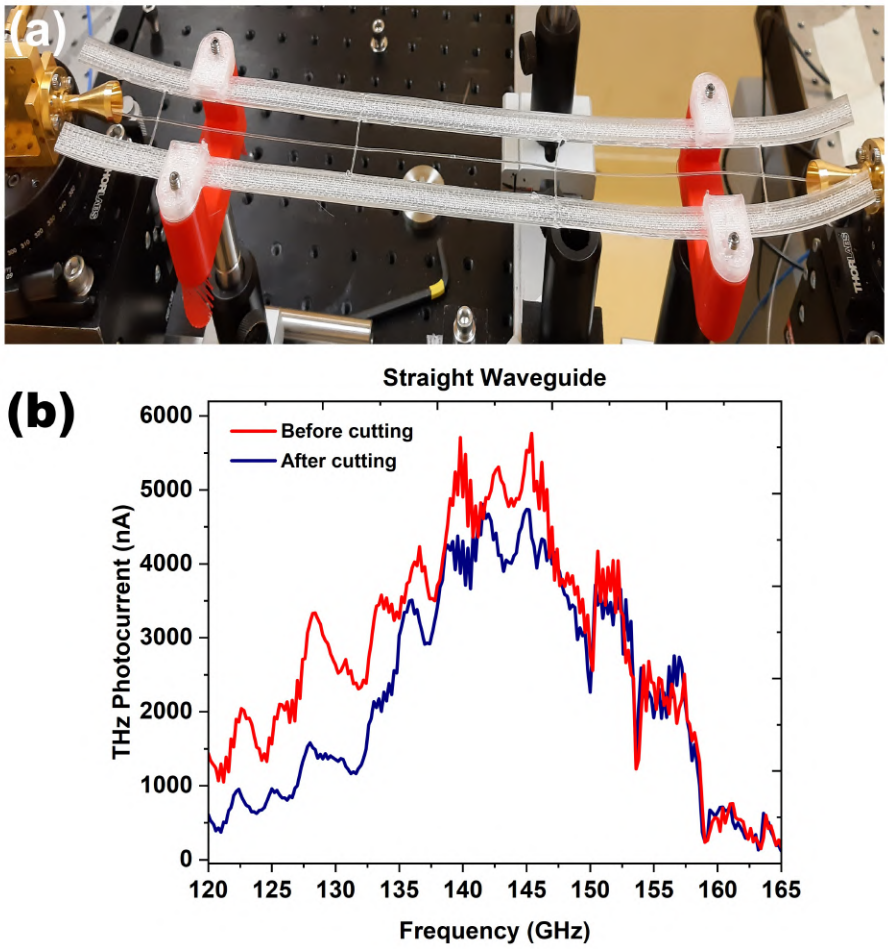

Figure 6.2 (a)Photo of the straight waveguide with the experimental setup. (b) Measured spectra of the straight waveguide before and after cutting.

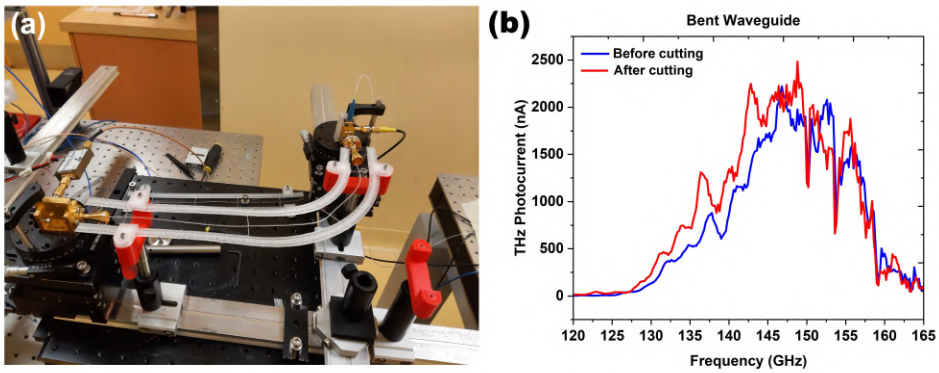

Figure 6.3 (a)Photo of the bent waveguide with the experimental setup. (b) Measured spectra of the bent waveguide before and after cutting.

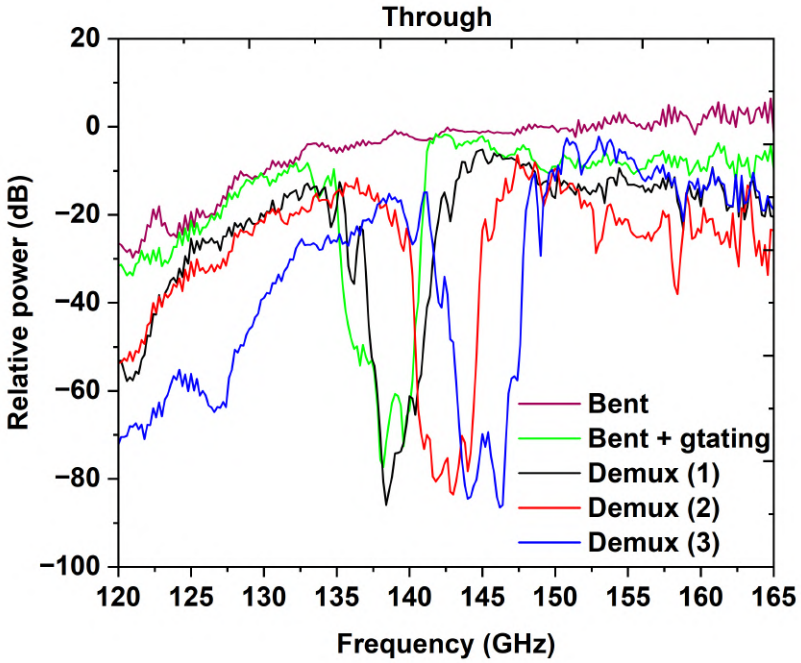

Figure 6.4 Measured relative transmission at the Through port.

the Through port exhibits a minimum, confirming efficient transfer of power from the input waveguide to the drop waveguide within the Bragg stopband. Outside these bands, the Drop transmission falls by more than 30–40 dB, indicating strong spectral selectivity and low crosstalk between adjacent THz WDM channels.

6.5 Future continuation of the project

The future continuation of this project holds significant promise for advancing terahertz (THz) communication systems and developing new capabilities within this emerging field. While the current research has laid a solid foundation by demonstrating 3D-printed terahertz demultiplexers using suspended-in-air grating couplers, several avenues remain for further improving and expanding the scope of this work. One key direction for continuing the project is refining the fabrication process. While polypropylene was a suitable choice due to its refractive index contrast and low absorption losses in the THz range, exploring new materials with even better THz transparency and lower loss characteristics could be highly beneficial. Materials such as polytetrafluoroethylene (PTFE) or polyvinyl alcohol (PVA) may offer better performance for terahertz waveguides and gratings. Additionally, improving the resolution of the 3D printing process could significantly enhance the precision of the fabricated

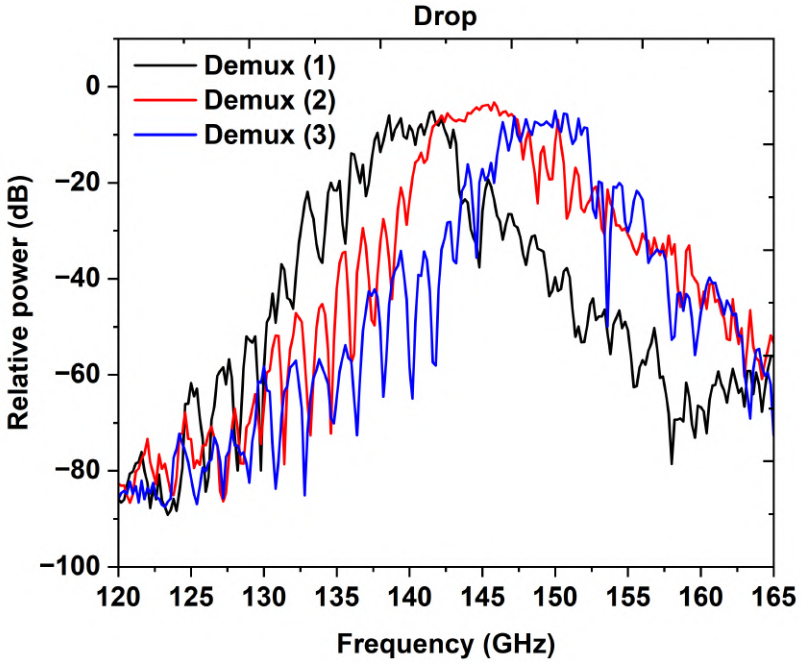

Figure 6.5 Measured relative power at the Drop ports.

components. Technologies such as stereolithography (SLA) or two-photon polymerization could provide the necessary resolution to create finer features and more intricate geometries, leading to more compact and efficient devices.

Further work will also focus on expanding the devices' functionality. Currently, the three-channel demultiplexer demonstrates the potential of 3D-printed THz components. However, as demand for higher bandwidth increases, there will be a need to develop devices capable of handling more channels. Scaling up the number of channels in a single device will require optimizing the design of grating couplers and waveguide networks to ensure efficient signal separation without introducing significant loss. Multi-channel demultiplexers will play a crucial role in facilitating higher data rates, so the next step will be to design and prototype five- or seven-channel demultiplexers, which could become essential for future terahertz communication systems. Moreover, increasing the data rates beyond the 6 Gbps demonstrated in this project will be a key objective. Achieving error-free transmission at even higher bit rates is a challenging yet necessary goal for terahertz systems aiming to meet the demands of future wireless networks. To achieve this, the focus will be on improving the signal-to-noise ratio (SNR) and addressing the bit error rate (BER) performance of the devices. By enhancing the precision of printed components and optimizing the overall system design, it

should be possible to achieve higher data rates while maintaining low error rates. Beyond integrating passive devices, there is a clear opportunity to incorporate active elements, such as optical amplifiers or modulators, into the printed structures. These active components could enhance the demultiplexer's capabilities, enabling the device to perform more complex tasks, such as signal modulation, amplification, and even frequency conversion. By integrating these active elements, we could move closer to achieving a fully integrated photonic circuit for THz communication, thereby significantly improving system performance while reducing manufacturing complexity and cost. The practical deployment of these devices will also require testing and validation across a broader range of real-world environments. While the experimental results obtained so far have shown promising performance in controlled lab conditions, the next step will be to test the devices in more challenging operational scenarios. This includes testing the devices under varying temperature conditions, over longer transmission distances, and with more complex signal environments. Real-world testing will provide critical insights into how these devices perform under the unpredictability of real communication channels and how they hold up in systems with higher channel densities and longer transmission ranges. Moreover, the scalability of the manufacturing process will be a critical focus in the future. Although the 3D printing approach demonstrated in this project is cost-effective and suitable for rapid prototyping, scaling up production for commercial applications will require standardizing the manufacturing process and materials. Future work will include developing standards for the fabrication of 3D-printed THz components to ensure consistency and establish a pathway for large-scale production. Collaboration with industry partners, particularly those in telecommunications and electronics manufacturing, will be key to advancing these devices from experimental prototypes to market-ready products.

CHAPTER 7 CONCLUSION

This research has successfully established a foundational framework for applying additive manufacturing to the development of high-performance, integrated terahertz communication devices. The work culminated in the design, fabrication, and comprehensive characterization of functional three-channel wavelength-division-multiplexing (WDM) demultiplexers, demonstrating the significant potential of 3D printing as a viable, disruptive technology for terahertz photonics. The core innovation lies in exploiting the high refractive index contrast provided by polypropylene filaments suspended in air. This material system enabled the realization of compact, low-loss waveguides, bends, couplers, and the critical Bragg grating filters that form the heart of the demultiplexing function. The use of a dual-nozzle FDM printer was pivotal, allowing the simultaneous deposition of 800µm filaments for structural waveguides and 400µm filaments for defining high-quality Bragg gratings with up to 100 periods. Additionally, the development of a specialized mechanical support structure and a novel low-loss splicing technique using a heated glass capillary was essential for integrating individual components into complex, functional devices—a challenge commonly encountered in suspended architectures.

The process from numerical design to experimental validation proved highly successful. Finite element simulations in COMSOL Multiphysics were used to optimize three distinct demultiplexer designs targeting drop channels at 138 GHz, 142 GHz, and 146 GHz within the 120–165 GHz band. Experimental results closely matched these theoretical predictions, confirming the intended operational principles. The devices successfully separated terahertz channels, with measured performance metrics that were not only functional but, in some aspects, superior to simulations. Notably, the experimental Drop port bandwidth was approximately 6 GHz, broader than the predicted 4 GHz, and exhibited excellent sidelobe suppression, which is critical for minimizing inter-channel crosstalk in dense WDM systems. Importantly, bit-error-rate (BER) characterization confirmed the devices' ability to handle high-speed data, achieving error-free operation (BER $< 10^{12}$) on individual channels at data rates up to 6 Gbps. This performance, demonstrated for both standalone filters and their combinations in sequential and parallel configurations, validates the practical applicability of these 3D-printed components in real-world terahertz communication links. The estimated insertion losses of 1.7dB for the Drop port and 1dB for the Through port further indicate that a system with ten or more sequentially placed channels is feasible within a reasonable power budget.

Despite the overall success, a critical analysis reveals specific discrepancies that point to opportunities for future improvement. The experimental spectra consistently showed deviations of several gigahertz compared to the simulations, and the maximum transmission amplitudes at the Drop ports were measured between 0.5 and 0.6, lower than the theoretical value of 0.8. These discrepancies are primarily attributed to scattering losses from the necessary mechanical support structures, numerically estimated at approximately 10% per support, as well as other inherent imperfections of the FDM printing process, such as waveguide wall roughness and micro-bending. While these factors did not prevent the successful demonstration of the devices, they underscore the primary challenge of this fabrication approach: balancing mechanical stability with optical performance.

Nevertheless, this work demonstrates that additive manufacturing with high-refractive-index-contrast material combinations, such as polypropylene-in-air, offers a highly viable and promising pathway for rapid prototyping and the development of integrated terahertz devices. The ability to transition from a digital model to a fully characterized, high-performance optical device in a matter of hours at a fraction of the cost of cleanroom fabrication represents a significant advantage. This accessibility can accelerate innovation in THz research, enabling rapid iteration of complex designs, including three-dimensional integrated circuits that are difficult or impossible to achieve with traditional planar lithography. These suspended-in-air integrated terahertz circuits hold immense potential for developing a broader class of linear optical transformers, which will be key to energy-efficient analog processing of data streams in the emerging terahertz communications system.

Looking ahead, this research points to several promising directions for future work. The immediate priority should be to mitigate the identified losses and imperfections, which could involve exploring advanced 3D printing technologies such as stereolithography (SLA), which offer superior surface finish and dimensional accuracy and potentially eliminate the need for support structures. Investigating alternative THz-transparent polymer materials with lower intrinsic absorption or improved printability is also recommended. To address spectral shifts and enhance functionality, integrating active tuning mechanisms is a critical next step. Building on concepts from tunable polymer Bragg gratings, incorporating micro-heaters could enable post-fabrication trimming of the Bragg wavelength and dynamic channel selection, compensating for fabrication tolerances and adding new functionality.

The next stage involves designing and fabricating demultiplexers with higher channel counts (e.g., 8 or 16 channels) and reduced channel spacing to maximize spectral efficiency. Achieving this will require more sophisticated grating designs, such as apodized or phase-shifted gratings, to improve roll-off and minimize crosstalk. Finally, to transition from prototypes

to deployable systems, efforts must focus on system-level integration and packaging. This includes developing standardized, low-loss interfaces between 3D-printed circuits and conventional THz hardware, such as horn antennas and waveguide flanges, and ultimately demonstrating a complete THz communication link with a printed multiplexer at the transmitter and a printed demultiplexer at the receiver, handling real multi-channel data traffic. Pursuing these directions will fully realize the potential of low-cost, rapidly prototyped, high-performance terahertz integrated circuits, cementing the role of additive manufacturing in advancing 6G and future wireless communication technologies. In conclusion, 3D printing (additive manufacturing) offers a range of intrinsic advantages, including the ability to fabricate complex geometries, compatibility with diverse materials (including metals, plastics, and ceramics), high dimensional precision, cost efficiency through reduced material waste, and the effective production of intricate structures. These strengths greatly facilitate the manufacturing of optical fibers and waveguides with complex designs. With continued advancements in 3D printing technologies, it is expected that increasingly sophisticated THz demultiplexers, waveguides, fibers, and functional devices will transition from theoretical concepts to practical realizations.

REFERENCES

[1] B. Ferguson et X.-C. Zhang, "Materials for terahertz science and technology," *Nature materials*, vol. 1, n°. 1, p. 26–33, 2002.

[2] T. Kleine-Ostmann et T. Nagatsuma, "A review on terahertz communications research," *Journal of Infrared, Millimeter, and Terahertz Waves*, vol. 32, n°. 2, p. 143–171, 2011.

[3] H. Gao *et al.*, "3d printed optics and photonics: processes, materials and applications," *Materials today*, vol. 69, p. 107–132, 2023.

[4] A. B. Icli *et al.*, "Numerical and experimental demonstration of inverse designed low-index polarization-insensitive wavelength demultiplexer," *Journal of Physics D: Applied Physics*, vol. 54, n°. 50, p. 505102, 2021.

[5] D. K. Gayen, "Optical multiplexer," *Journal of Mechanics of Continua and Mathematical Sciences*, vol. 18, n°. 3, p. 32–42, 2023.

[6] G. E. Keiser, "A review of wdm technology and applications," *Optical Fiber Technology*, vol. 5, n°. 1, p. 3–39, 1999.

[7] M. Mishra et P. K. Sahu, "A study on apodization profiles of fiber bragg gratings," dans *Advances in Intelligent Computing and Communication: Proceedings of ICAC 2021*. Springer, 2022, p. 183–189.

[8] Raise3D. (n.d.) Raise3d pro2 3d printer. [En ligne]. Disponible: https://www.raise3d.com/products/raise3d-pro2-3d-printer/

[9] B. Yahyapour *et al.*, "Terahertz demultiplexrs suspended in air using 3d printing technique," dans *2025 IEEE 15th Annual Computing and Communication Workshop and Conference (CCWC)*. IEEE, 2025, p. 01 021–01 023.

[10] ——, "3d printed thz demultiplexer circuits using suspended-in-air grating couplers," dans *2025 IEEE International Conference on Consumer Electronics (ICCE)*. IEEE, 2025, p. 1–3.

[11] D. M. Mittleman, "Perspective: Terahertz science and technology," *Journal of Applied Physics*, vol. 122, n°. 23, 2017.

[12] V. Rogalin, I. Kaplunov et G. Kropotov, "Optical materials for the thz range," *Optics and Spectroscopy*, vol. 125, n°. 6, p. 1053–1064, 2018.

[13] M. Nagel *et al.*, “Integrated thz technology for label-free genetic diagnostics,” *Applied Physics Letters*, vol. 80, nº. 1, p. 154–156, 2002.

[14] Z. Chen *et al.*, “A survey on terahertz communications,” *China communications*, vol. 16, nº. 2, p. 1–35, 2019.

[15] S. Cherry, “Edholm’s law of bandwidth,” *IEEE Spectrum*, vol. 41, nº. 7, p. 58–60, 2004.

[16] H. Song et T. Nagatsuma, “Present and future of terahertz communications,” *IEEE Transactions on Terahertz Science and Technology*, vol. 1, nº. 1, p. 256–263, 2011.

[17] J. Huang *et al.*, “Multi-frequency mmwave massive mimo channel measurements and characterization for 5g wireless communication systems,” *IEEE Journal on Selected Areas in Communications*, vol. 35, nº. 7, p. 1591–1605, 2017.

[18] J. Bae et Y. S. Choi, “System capacity enhancement of mmwave based 5g mobile communication system,” dans *International Conference on Information and Communication Technology Convergence (ICTC)*, 2015, p. 291–294.

[19] J. Zhang *et al.*, “6–100 ghz research progress and challenges from a channel perspective for fifth generation (5g) and future wireless communication,” *Science China Information Sciences*, vol. 60, nº. 8, p. 080301, 2017.

[20] T. S. Rappaport, J. N. Murdock et F. Gutierrez, “State of the art in 60-ghz integrated circuits and systems for wireless communications,” *Proceedings of the IEEE*, vol. 99, nº. 8, p. 1390–1436, 2011.

[21] S. K. Agrawal et K. Sharma, “5g millimeter wave (mmwave) communications,” dans *International Conference on Computing for Sustainable Global*, 2016.

[22] S. Mumtaz *et al.*, “Terahertz communication for vehicular networks,” *IEEE Transactions on Vehicular Technology*, vol. 66, nº. 7, p. 5617–5625, 2017.

[23] G. Xu et M. Skorobogatiy, “3d printing technique and its application in the fabrication of thz fibers and waveguides,” *Journal of Applied Physics*, vol. 133, nº. 21, 2023.

[24] K. Willis *et al.*, “Printed optics: 3d printing of embedded optical elements for interactive devices,” dans *Proceedings of the 25th annual ACM symposium on User interface software and technology*, 2012.

[25] N. Dudukovic *et al.*, “Additive manufacturing of lightweight mirrors,” dans *Dimensional Optical Metrology and Inspection for Practical Applications VII*. SPIE, 2018.

[26] S. Ford et T. Minshall, “Additive manufacturing,” *Additive Manufacturing*, vol. 25, p. 131–150, 2019.

[27] S. Derakhshanfar *et al.*, “Bioactive materials,” *Bioactive Materials*, vol. 3, nº. 2, p. 144–156, 2018.

[28] J. Gonzalez-Gutierrez *et al.*, “Materials,” *Materials*, vol. 11, nº. 5, 2018.

[29] J. Suszek *et al.*, “Evaluation of the shadow effect in terahertz<? a3b2 show [pmg: line-break justify=" yes"/]?> kinoform gratings,” *Optics letters*, vol. 38, nº. 9, p. 1464–1466, 2013.

[30] J. P. Ryan, “Wdm: North american deployment trends,” *IEEE Communications Magazine*, vol. 36, p. 40, 1998.

[31] E. Lowe, “Current european wdm deployment trends,” *IEEE Communications Magazine*, vol. 36, p. 46, 1998.

[32] B. K. Yıldırım *et al.*, “Numerical and experimental demonstration of inverse designed low-index polarization-insensitive wavelength demultiplexer,” *Journal of Lightwave Technology*, vol. 39, nº. 12, p. 4009–4017, 2021.

[33] G. R. Hill, “Wavelength domain optical network techniques,” *Proceedings of the IEEE*, vol. 78, p. 121, 1990.

[34] T. Miki, “Optical transport networks,” *Proceedings of the IEEE*, vol. 81, p. 1594, 1993.

[35] K. Nosu, *Optical FDM Network Technologies*. Boston: Artech House, 1997.

[36] M. J. O’Mahoney, “Optical multiplexing in fiber networks: Progress in wdm and otdm,” *IEEE Communications Magazine*, vol. 33, p. 82, 1995.

[37] W. J. Goralski, *SONET: A Guide to Synchronous Optical Network*. New York: McGraw-Hill, 1997.

[38] B. Yahyapour *et al.*, “3d-printed demultiplexer circuits using suspended-in-air grating couplers for terahertz communications,” *IEEE Access*, 2025.

[39] Y. Niu *et al.*, “A survey of millimeter wave communications (mmwave) for 5g: opportunities and challenges,” *Wireless networks*, vol. 21, nº. 8, p. 2657–2676, 2015.

[40] I. F. Akyildiz, J. M. Jornet et C. Han, “Terahertz band: Next frontier for wireless communications,” *Physical communication*, vol. 12, p. 16–32, 2014.

[41] S. Dang *et al.*, "From a human-centric perspective: What might 6g be?" *Authorea Preprints*, 2023.

[42] T. Nagatsuma, G. Ducournau et C. C. Renaud, "Advances in terahertz communications accelerated by photonics," *Nature Photonics*, vol. 10, nº. 6, p. 371–379, 2016.

[43] M. Poulin, S. Giannacopoulos et M. Skorobogatiy, "Surface wave enhanced sensing in the terahertz spectral range: Modalities, materials, and perspectives," *Sensors*, vol. 19, nº. 24, p. 5505, 2019.

[44] Y. Cao *et al.*, "Additive manufacturing of resonant fluidic sensors based on photonic bandgap waveguides for terahertz applications," *Optics Express*, vol. 27, nº. 20, p. 27 663–27 681, 2019.

[45] K. Fukunaga *et al.*, "Real-time terahertz imaging for art conservation science," *Journal of the European Optical Society-Rapid publications*, vol. 3, p. 08027, 2008.

[46] H. Guerboukha, K. Nallappan et M. Skorobogatiy, "Toward real-time terahertz imaging," *Advances in Optics and Photonics*, vol. 10, nº. 4, p. 843–938, 2018.

[47] Y. Shen *et al.*, "Detection and identification of explosives using terahertz pulsed spectroscopic imaging," *Applied physics letters*, vol. 86, nº. 24, 2005.

[48] J. F. Federici *et al.*, "Thz imaging and sensing for security applications—explosives, weapons and drugs," *Semiconductor science and technology*, vol. 20, nº. 7, p. S266, 2005.

[49] M. A. Akkaş, "Terahertz wireless data communication," *Wireless Networks*, vol. 25, nº. 1, p. 145–155, 2019.

[50] K. Nallappan *et al.*, "Live streaming of uncompressed hd and 4k videos using terahertz wireless links," *IEEE Access*, vol. 6, p. 58 030–58 042, 2018.

[51] S. Koenig *et al.*, "Wireless sub-thz communication system with high data rate," *Nature photonics*, vol. 7, nº. 12, p. 977–981, 2013.

[52] H. Elayan *et al.*, "Terahertz band: The last piece of rf spectrum puzzle for communication systems," *IEEE Open Journal of the Communications Society*, vol. 1, p. 1–32, 2019.

[53] H. Li *et al.*, "Longitudinal manipulation of scalar to vector vortex beams evolution empowered by all-silicon metasurfaces," *Advanced Optical Materials*, vol. 11, nº. 22, p. 2301368, 2023.

[54] ——, “Polarization detection of terahertz waves using all-silicon metasurfaces with tightly focusing behavior,” *Laser & Photonics Reviews*, vol. 17, n°. 12, p. 2300428, 2023.

[55] ——, “Broadband all-dielectric meta-lenses with terahertz full-stokes polarization detection behavior,” *Optics Express*, vol. 32, n°. 21, p. 37 916–37 927, 2024.

[56] A. Shafie *et al.*, “Terahertz communications for 6g and beyond wireless networks: Challenges, key advancements, and opportunities,” *IEEE Network*, vol. 37, n°. 3, p. 162–169, 2022.

[57] V. Petrov, T. Kurner et I. Hosako, “Ieee 802.15. 3d: First standardization efforts for sub-terahertz band communications toward 6g,” *IEEE Communications Magazine*, vol. 58, n°. 11, p. 28–33, 2020.

[58] M. Polese *et al.*, “Toward end-to-end, full-stack 6g terahertz networks,” *IEEE Communications Magazine*, vol. 58, n°. 11, p. 48–54, 2020.

[59] L. John *et al.*, “Broadband 300-ghz power amplifier mmics in ingaas mhemt technology,” *IEEE Transactions on Terahertz Science and Technology*, vol. 10, n°. 3, p. 309–320, 2020.

[60] X. Yu *et al.*, “160 gbit/s photonics wireless transmission in the 300-500 ghz band,” *APL Photonics*, vol. 1, n°. 8, 2016.

[61] T. Nagatsuma *et al.*, “300-ghz-band wireless communication using fermi-level managed barrier diode receiver,” dans *2019 IEEE MTT-S International Microwave Symposium (IMS)*. IEEE, 2019, p. 762–765.

[62] J. Kiegling *et al.*, “High power and spectral purity continuous-wave photonic thz source tunable from 1 to 4.5 thz for nonlinear molecular spectroscopy,” *New Journal of Physics*, vol. 15, n°. 10, p. 105014, 2013.

[63] N. Oshima *et al.*, “Terahertz wireless data transmission with frequency and polarization division multiplexing using resonant-tunneling-diode oscillators,” *IEEE Transactions on Terahertz Science and Technology*, vol. 7, n°. 5, p. 593–598, 2017.

[64] H. Zhao *et al.*, “Demonstration of orbital angular momentum multiplexing and demultiplexing based on a metasurface in the terahertz band,” *ACS Photonics*, vol. 5, n°. 5, p. 1726–1732, 2017.

[65] Q. Wang *et al.*, “Polarization and frequency multiplexed terahertz meta-holography,” *Advanced Optical Materials*, vol. 5, n°. 14, p. 1700277, 2017.

[66] S. Jia *et al.*, “0.4 thz photonic-wireless link with 106 gb/s single channel bitrate,” *Journal of Lightwave Technology*, vol. 36, n°. 2, p. 610–616, 2018.

[67] ——, “Integrated dual-dfb laser for 408 ghz carrier generation enabling 131 gbit/s wireless transmission over 10.7 meters,” dans *Optical Fiber Communication Conference*. Optica Publishing Group, 2019, p. Th1C–2.

[68] K. Liu *et al.*, “100 gbit/s thz photonic wireless transmission in the 350-ghz band with extended reach,” *IEEE Photonics Technology Letters*, vol. 30, n°. 11, p. 1064–1067, 2018.

[69] W. Deng *et al.*, “On-chip polarization-and frequency-division demultiplexing for multidimensional terahertz communication,” *Laser & Photonics Reviews*, vol. 16, n°. 10, p. 2200136, 2022.

[70] N. Joshi et N. P. Pathak, “Tunable wavelength demultiplexer using modified graphene plasmonic split ring resonators for terahertz communication,” *Photonics and Nanostructures-Fundamentals and Applications*, vol. 28, p. 1–5, 2018.

[71] U. H. Fischer *et al.*, “Polymeric demultiplexer component for wavelength division multiplex communication systems using polymer fibers,” dans *Optical Interconnects XV*, vol. 9368. SPIE, 2015, p. 167–177.

[72] M. Haupt et U. Fischer, “Optical design of a low-loss demultiplexer for optical communication systems in the visible range,” dans *Optical Systems Design 2012*, vol. 8550. SPIE, 2012, p. 166–173.

[73] M. S. Borella *et al.*, “Optical components for wdm lightwave networks,” *Proceedings of the IEEE*, vol. 85, n°. 8, p. 1274–1307, 1997.

[74] L. Smith *et al.*, “Characterization of a split-ring-resonator-loaded transmission line at terahertz frequencies,” *Optics Express*, vol. 29, n°. 15, p. 23 282–23 289, 2021.

[75] S.-Y. Chiam *et al.*, “Increased frequency shifts in high aspect ratio terahertz split ring resonators,” *Applied Physics Letters*, vol. 94, n°. 6, 2009.

[76] T. Driscoll *et al.*, “Tuned permeability in terahertz split-ring resonators for devices and sensors,” *Applied Physics Letters*, vol. 91, n°. 6, 2007.

[77] F. Ma *et al.*, “Tunable multiband terahertz metamaterials using a reconfigurable electric split-ring resonator array,” *Light: Science & Applications*, vol. 3, n°. 5, p. e171–e171, 2014.

[78] G.-B. Wu *et al.*, "3-d-printed terahertz metalenses for next-generation communication and imaging applications," *Proceedings of the IEEE*, 2024.

[79] F.-S. Hsiao *et al.*, "A 5g/terahertz integrated wireless network based on wavelength-division multiplexing and terahertz photomixing," dans *2021 46th International Conference on Infrared, Millimeter and Terahertz Waves (IRMMW-THz)*. IEEE, 2021, p. 1–2.

[80] H. Xin et M. Liang, "3-d-printed microwave and thz devices using polymer jetting techniques," *Proceedings of the IEEE*, vol. 105, n°. 4, p. 737–755, 2017.

[81] J. Chen *et al.*, "3d-printed anisotropic polymer materials for functional applications," *Advanced Materials*, vol. 34, n°. 5, p. 2102877, 2022.

[82] Y. Cao *et al.*, "Add drop multiplexers for terahertz communications using two-wire waveguide-based plasmonic circuits," *Nature Communications*, vol. 13, n°. 1, p. 4090, 2022.

[83] J. Li *et al.*, "3d printed hollow core terahertz bragg waveguides with defect layers for surface sensing applications," *Optics Express*, vol. 25, n°. 4, p. 4126–4144, 2017.

[84] M. Ortiz-Martinez, E. Castro-Camus et A. Hernandez-Serrano, "Guided-mode filters for terahertz frequencies fabricated by 3d printing," *Journal of Infrared, Millimeter, and Terahertz Waves*, vol. 40, p. 731–737, 2019.

[85] M. Weidenbach *et al.*, "3d printed dielectric rectangular waveguides, splitters and couplers for 120 ghz," *Optics Express*, vol. 24, n°. 25, p. 28 968–28 976, 2016.

[86] D. Jahn *et al.*, "3d printed terahertz focusing grating couplers," *Journal of Infrared, Millimeter, and Terahertz Waves*, vol. 38, p. 708–716, 2017.

[87] J. Ma *et al.*, "Communications with thz waves: switching data between two waveguides," *Journal of Infrared, Millimeter, and Terahertz Waves*, vol. 38, p. 1316–1320, 2017.

[88] J.-S. Li, L. Han et Z. Le, "Compact four-channel terahertz demultiplexer based on directional coupling photonic crystal," *Optics Communications*, vol. 350, p. 248–251, 2015.

[89] W. Pan *et al.*, "A terahertz demultiplexer based on metamaterials applied to terahertz communication systems," *Progress in Electromagnetics Research Letters*, vol. 97, p. 13–19, 2021.

[90] G. Yan *et al.*, "Low-loss terahertz waveguide bragg grating using a two-wire waveguide and a paper grating," *Optics Letters*, vol. 38, nº. 16, p. 3089–3092, 2013.

[91] J. Yuan *et al.*, "Terahertz filters based on subwavelength polymer waveguide," *Results in Physics*, vol. 13, p. 102198, 2019.

[92] M. Burla *et al.*, "Integrated waveguide bragg gratings for microwave photonics signal processing," *Optics Express*, vol. 21, nº. 21, p. 25 120–25 147, 2013.

[93] M. A. Butt, N. L. Kazanskiy et S. N. Khonina, "Advances in waveguide bragg grating structures, platforms, and applications: an up-to-date appraisal," *Biosensors*, vol. 12, nº. 7, p. 497, 2022.

[94] M.-C. Oh *et al.*, "Tunable wavelength filters with bragg gratings in polymer waveguides," *Applied Physics Letters*, vol. 73, nº. 18, p. 2543–2545, 1998.

[95] O. S. Carneiro, A. Silva et R. Gomes, "Fused deposition modeling with polypropylene," *Materials & Design*, vol. 83, p. 768–776, 2015.